Approved for Public Release;
Distribution Unlimited.

ENVPREDRSCHFAC
Technical Note No. 4-74

COMPUTATION OF TIDES, CURRENTS, AND DISPERSAL OF POLLUTANTS IN THE NEW YORK BIGHT FROM BLOCK ISLAND TO ATLANTIC CITY WITH LARGE GRID SIZE, SINGLE AND TWO-LAYER HYDRODYNAMICAL-NUMERICAL MODELS

By

T. LAEVASTU and R. CALLAWAY

in collaboration with

A. STROUD and M. CLANCY

Part 4 of a series of four reports

Prepared for

ENVIRONMENTAL PROTECTION AGENCY
PACIFIC NORTHWEST ENVIRONMENTAL
RESEARCH LABORATORY
CORVALLIS, OREGON

JANUARY 1974

ENVIRONMENTAL PREDICTION RESEARCH FACILITY
NAVAL POSTGRADUATE SCHOOL
MONTEREY, CALIFORNIA 93940

REPORT DOCUMENTATION PAGE		READ INSTRUCTIONS BEFORE COMPLETING FORM
1. REPORT NUMBER ENVPREDRSCHFAC Technical Note No. 4-74	2. GOVT ACCESSION NO.	3. RECIPIENT'S CATALOG NUMBER
4. TITLE (and Subtitle) Computation of Tides, Currents and Dispersal of Pollutants in the New York Bight from Block Island to Atlantic City with Large Grid Size, Single and Two-Layer Hydrodynamical-Numerical Models		5. TYPE OF REPORT & PERIOD COVERED 6. PERFORMING ORG. REPORT NUMBER
7. AUTHOR(s) T. Laevastu and R. Callaway with A. Stroud and M. Clancy		8. CONTRACT OR GRANT NUMBER(s)
9. PERFORMING ORGANIZATION NAME AND ADDRESS Environmental Prediction Research Facility Naval Postgraduate School Monterey, California 93940		10. PROGRAM ELEMENT, PROJECT, TASK AREA & WORK UNIT NUMBERS
11. CONTROLLING OFFICE NAME AND ADDRESS Naval Air Systems Command Department of the Navy Washington, D.C. 20361		12. REPORT DATE January 1974 13. NUMBER OF PAGES 84
14. MONITORING AGENCY NAME & ADDRESS (if different from Controlling Office)		15. SECURITY CLASS. (of this report) UNCLASSIFIED 15a. DECLASSIFICATION/DOWNGRADING SCHEDULE

16. DISTRIBUTION STATEMENT (of this Report)

Approved for Public Release; Distribution Unlimited.

17. DISTRIBUTION STATEMENT (of the abstract entered in Block 20, if different from Report)

18. SUPPLEMENTARY NOTES

19. KEY WORDS (Continue on reverse side if necessary and identify by block number)

Hydrodynamical-Numerical Model
Computation of tide and currents
Dispersal of pollutants
New York Bight

20. ABSTRACT (Continue on reverse side if necessary and identify by block number)

The application of a large grid HN model to the New York Bight is to large extent a problem of treating two long open boundaries. The input at these open boundaries serves also for tuning of the results inside the computational area.

A few earlier current measurements by two lightships in the Bight as reported by Haight (1942) have been used for verification. The tidal currents predominate in the New York Bight

20. (Continued)

proper, with a superimposed slow net flow toward the south. This net flow can be simulated in the models and tuned with the prescription of a proper slope to the two open boundaries.

The diffusion computations over a short period of time in the large grid models do not give fully satisfactory results with the diffusion model used at present in the HN models, instead, the transport of the centers of release points have been computed and presented. Furthermore, the net transport through various sections in the area has also been computed. The single-layer model is applicable for the winter season when the area is fully mixed from surface to the bottom.

In the two-layer HN model, which is applicable for summer conditions when stratification of the waters occurs, some inputs such as internal friction, need some additional numerical experimentation and adjustment and above all proper field measurements as nearly no data is available for the selection of a proper internal friction coefficient. Furthermore, internal waves (internal fluctuations) occur in the interface after introduction of the wind into the model run. These fluctuations diminish with time, and subsequently require a longer real-time computation period and as a consequence, more computer time. Such fluctuations are known to occur in the sea as recordings of thermal structure changes with depth and time over the continental shelf, as well as sea-level recordings near the coasts have shown.

Of practical importance is the knowledge of differences in the currents in upper and lower layers and the time and space variation of these differences. The results of the model show that in many areas a different net flow occurs in the lower layer than in the surface layer. This is partly demonstrated in the report with some of the output from special selected points and agrees with the results from sea-bed drifter experiments.

There is a coastward movement of the deeper layers off Long Island Sound, making this area less desirable for sludge disposal. The Hudson Submarine Canyon divides the hydrographic regime in New York Bight. The flow south of the canyon is stronger and toward the south. A potential use of this type of study is in the selection of general areas where sludge dumping may be less troublesome than in others.

FOREWORD

This report describes the results of the application of Hydrodynamical-Numerical (HN) models to New York Bight. The results of computer runs with a large, two-open boundary, single-layer model, as well as with a two-layer model for the same area, are presented. Many of the problems in the application of these models are connected with the treatment of the open boundaries. The Environmental Prediction Research Facility (EPRF) has found a few satisfactory methods for the treatment of these boundaries, some of which are briefly mentioned in this report. The method is further described in Part 2 of the report series where the two-layer model is documented (see references).

Verification of the New York Bight models is very brief, due to scarcity of proper observations. However, the models have been verified in other applications, to the extent that they are considered to be ready for operational and real-time use. It could be mentioned that a 3-layer version of the models have now been applied at EPRF to larger open ocean areas with considerable success. The experiences from these applications have been indirectly used in this work and are available to EPA.

CONTENTS

LIST OF FIGURES

LIST OF FIGURES (cont.)

LIST OF FIGURES (cont.)

LIST OF FIGURES (cont.)

LIST OF FIGURES (cont.)

I. INTRODUCTION

One of the limiting problems in the past, in the application of HN models off the open coasts has been the difficulty of treating several open boundaries. Considerable efforts has been made at EPRF for over two years to devise methods to solve this problem. Two methods have been found to be relatively satisfactory for this purpose (see part 2 in this report series). These methods have been applied and tested further in the application of HN models to the New York Bight, which are described in this report.

This report describes the application and the results of a single-layer and a two-layer HN model with several open boundaries. Many applied problems in estuaries and off coasts in stratified conditions require the use of at least a two-layer HN model, as different movements and transports occur in different layers with the presence of sharp thermocline and/or pycnocline. This condition in turn has profound influence on the transport of polluted waters, in the design of waste water outlets, and in the selection of waste disposal areas.

Only essential results of the numerical computations are described and summarized in this report. A voluminous amount of numerical data created by these models will be available at the EPA laboratory in Corvallis. Furthermore, these models, especially the two-layer models, have a great number of various application possibilities all of which could not be foreseen, demonstrated, or explored within this project.

Finally, it should be mentioned that one of the limiting factors in the application of the two-layer model (as, indeed, in all numerical experimentation) is the computer cost. This model requires a large computer with a relatively large core and long computation times due to the short time steps dictated by numerical stability. Various investigations are in progress

to find ways to decrease the time step by applying, e.g., both an explicit and an implicit method simultaneously for solution of the equations. Further reports will be forthcoming in this subject as well as on the comparison of various methods on computational application of hydrodynamical methods.

2. SINGLE-LAYER, LARGE GRID SIZE MODEL FOR NEW YORK BIGHT AND LONG ISLAND SOUND

2.1 INPUTS INTO THE MODEL

The grid net for the large scale New York Bight model and the locations of special output points and sections are shown in Figure 1. This model was run with two open boundaries. The area was predetermined and the grid net selected so that the model could be run on CDC 7600 computer without large core memory. The grid size thus became 6.556 km and the corresponding time step dictated by stability criterium was 30 sec.

Each input of tide was made with four tidal constituents. The tidal amplitudes and phases were interpolated along the imput boundaries from the harmonic constants of Atlantic City and those of Montauk Point. The time difference between these two stations was ascertained, and the difference was extrapolated over the input boundary to derive a realistic time difference at the seaward corner of the grid. Some additional adjustment was made at the southernmost end of the input boundary off Atlantic City. This was necessary to effect the net flow along the continental shelf in this area. The winds used were the same typical summer and winter winds as used in smaller scale models (see part 3 of this report series).

2.2 TIDES

A comparison of the tides computed with HN models and the harmonic tides at Sandy Hook are given in Figure 2. Sandy Hook is located a considerable distance from the boundaries. As is apparent from this figure, it will take the model about 12 hours to reach the proper equilibrium with the tides at this location. After equilibrium is reached, the HN computed and harmonic tides are in good agreement.

Callaway (unpubl.) has made measurements with deep sea tide gauges at 39°37.5'N; 73°42.0'W (off Barnegat Inlet) and at 40°27.8'N and 71°28.4'W (South of Montauk Point). Some of his data on amplitudes of tidal constituents are given in Table 1 together with available data from International Hydrographic Bureau's (IHB) tidal constituent sheets.

Table 1. Amplitudes of tides (cm) from IHB tidal constituent list and as measured with deep sea tide gauge by Callaway (unpublished).

Constituent	M_2	S_2	N_2	K_1	O_1
39°37.5'N, 73°42.0'W (Callaway)	54.8	10.8	12.4	10.3	7.2
39°21'N, 74°26'W (IHB, No. 507)	58.3	11.9	13.7	10.3	7.7
40°27.8'N, 71°28.4'W (Callaway	43.0	8.6	8.4	6.6	3.7
41°03'N, 71°58'W (IHB, No. 2213)	28.3	6.9	7.7	6.6	5.0

Taking into consideration the distances between the locations, there is a good agreement between Callaway's and IHB data, with exception of M_2 amplitude off Montauk Point. Considering other tidal data from New York Bight area, there is reason to believe that IHB amplitude for M_2 tide at Montauk Point is in error. The IHB data were used in the model run, as Callaway data became available later.

The sea level and currents at Points 5 and 10 (for location see Figure 1) are shown in Figures 3 and 4. A comparison of these figures shows that the tidal amplitudes decrease somewhat from the coast to offshore (as is known from empirical observations). The rate of decrease is variable and depends on several factors, including the change of depth and slope of the bottom.

2.3 CURRENTS

Figures 5 to 15 show the current ellipses at various output points (for locations, see Figure 1). These figures serve to illustrate the nature of tidal currents and their variations. When accurate data are required, e.g., the relation between the direction of the current to the tidal amplitude stage, they can be extracted from printouts. Nearly every point has certain local peculiarities. Figure 5 shows the reversing (back-and-forth) tide at the mouth of the Ambrose Channel. A comparison of the current speeds with those at Point 5 (Figure 6) reveals the pronounced effect of the channel on the currents. Figure 7 shows the currents somewhat closer to the coast and in shallower water than those shown in Figure 6, and indicates the slightly stronger currents in this location (as expected from empirical knowledge). Comparisons of Figure 9 (Point 13) with Figures 10 (Point 18) and 11 (Point 19) demonstrates the widening of the tidal ellipses to nearly circular tides at Point 20 (Figure 12) further offshore.

Figure 14 shows a comparison of mean tidal currents at Scotland Lightship (Haight, 1942) and the currents computed at the nearest grid point (22,37 in Figure 1).

As can be recognized from this figure, the current directions and speed of computed currents are in reasonable agreement with the measured currents at the Lightship. The special output Point 4 in Ambrose Channel (see Figure 4 for location), from which the currents are presented on Figure 5, is about 9.3 km from Point 22,37 (grid coordinates) from which the currents are presented on Figure 16B. Comparison of the two figures (15 and 16B) indicates again, relatively great changes of currents over a relatively short distance.

Another comparison of measured and computed currents can be made at Fire Island Lightship (40°25'N; 73°11'W; Point IV on Figure 1) with currents extracted from a nearby grid point (Point 10 in Figure 1, for which currents are given in Figure 8).

According to Haight (1942) the mean flood at Fire Island Lightship is 0.23 kt to 96°. Converting the mean speeds given by Haight (1942) to the strength of currents, results 18 cm sec^{-1}. Figure 8 gives approximately the same directions, (85°) but the strength of the computed current is about 25 cm sec^{-1}. However, the currents presented in Figure 8 are tidal currents during spring tides, thus should be somewhat stronger than the strength of the current at mean tides.

Snapshot pictures of the distribution of current directions and speeds during different stages of the tides are shown in Figures 17 to 22. Figure 17 shows the currents during low water at Sandy Hook, and Figure 18 shows the currents two hours later at the start of flooding current. Figure 19 shows the currents two hours before high water at Sandy Hook. The essential feature of this figure is the strong inflow into the New York Bight in the region of the Hudson Submarine Canyon (bathymetry, see Figure 69) and the turning of this coastward flow south toward Atlantic City. Figure 20 shows the currents during near-slack water at Sandy Hook, which is the high water time at this location. The effect of Hudson Submarine Canyon is also clearly depicted on this figure. This figure depicts best the bifurcation of the currents near the head of Hudson Canyon, mentioned in a NOAA (1972) report. Figure 21 shows the beginning of the ebbing current, and an additional shapshot picture of the ebbing current 2 hours later is given in Figure 22. These two last figures show a slight intrusion of water in the deeper part of Hudson Submarine Canyon and the nearly continuous southward flow off Atlantic City.

The net currents after a full tidal cycle with southwest winds of 9 m sec^{-1} are shown in Figure 23. The stronger currents around the Hudson Submarine Canyon and off Atlantic City are essential features of this figure.

The recent measurements of McClennen (1973) of tidal currents 1.5 to 2.0 m above the bottom off the New Jersey coast show that the mean speeds are on the order of 15 cm sec^{-1}, with a maximum speed 40 cm sec^{-1} and that there is a net transport to the SW at the continental slope. The results of these measurements are in good general agreement with the computed currents in the SW corner of the computational grid.

Figure 23 also shows the net circulation in the New York Bight in good agreement with the results of drift bottle studies of Powers (1951). The essential features of this net circulation are: (a) a weak westerly flow in the central part of the Bight turning towards stronger southerly flow off the New Jersey coast; (b) main inflow along the Hudson Submarine Canyon (and south of it) and a weaker inflow from the east; (c) a weak towards-the-coast flow off the eastern part of Long Island, and (d) a net flow from Long Island Sound through the East River and Lower Bight.

Nontidal (net) currents at various lightship stations are shown in Figure 24 according to Haight (1942). These relatively incomplete data indicate the same circulation pattern as described above.

2.4 THE TRANSPORT OF WATER THROUGH VARIOUS SECTIONS

The transport rate of water ($m^3 sec^{-1}$) through a few sections are presented in Figures 25 to 28 as examples. The transport has been computed at each time step, using current components perpendicular to the section at each grid point and averaged hourly. Of greater interest are Figures 29 to 32 showing the net transport (accumulative net transport) through the given sections. A tendency of the change of net transport with time is apparent on these figures, which is due to several factors, such as the change of tides from spring towards neap tides and wind. Such a transport change has been empirically observed and is physically explainable, but has

not been underlined in past literature. The transport computations through predetermined sections within a tidal cycle can be used for computation of half-life of the water in various sub-areas (i.e., the flushing times) using the total volume of the water inside the areas bounded by sections. The flushing times vary considerably from one area to another as well as with the stage of tides and especially with the winds. A separate study and report is planned in this subject in the continuation of this project. Only a preliminary estimate was made with the transport computations at hand, which indicated that the Bight is flushed by net circulation in about each two weeks. This estimate is in general agreement with estimates by Ketchum, et al (1951) and Horne (1971).

2.5 DISPERSION AND DIFFUSION OF POLLUTANTS

Attempts were made to compute the dispersion and diffusion of "pollutants" in this model with the same formulation as in the small grid model and the concentrations through a full tidal cycle after release are shown in Figure 33. However, certain limitations of this approach in large-grid size models are apparent, especially with respect to the movement of the central values of the "blobs". The main limitation of diffusion and dispersion computations with the Lagrangian method is that the grid size should be smaller than half of the distance of tidal excursion. The excursion of the centers of the "original releases" (blobs) at various points were computed and the results are given in Figures 34 to 42. The release was affected at the grid point shown with the crossed lines on the figures. The numbers on these grid lines indicate the tenths of grid size. The central position of the blob is given for each 2 hours. Furthermore, the net transport (the difference between the original position and the position after a full tidal cycle) is shown with a thick dashed line on these figures. Detailed evaluation of the water (and pollution) movement, and

comparison of the movement, in various parts of the Bight can be obtained by comparing these figures. It should be noted that, besides the variation of the magnitude of "tidal excursion", the selected release points fall into two categories: (a) those with little or no net transport showing the movement of a particle in a tidal ellipse (e.g., Figures 34 and 39) and (b) those with considerable net transport after a full tidal cycle. (e.g., Figures 38 and 42).

3. TWO-LAYER, LARGE GRID SIZE MODEL FOR THE NEW YORK BIGHT

3.1 SEA LEVEL AND MIXED LAYER DEPTH

The computational grid for the two-layer model and the special output points are the same as for the single-layer large scale model (Figure 1).

A comparison of the tides computed with the harmonic method and those computed with the two-layer HN model at Sandy Hook is given in Figure 43. First, it will be noticed that it will take more than 12 hours to achieve computational equilibrium, as was the case with the single-layer, large-grid size model. Furthermore, after about 22 hours, the tides computed with two-layer HN model do not follow well the harmonic tidal curve, but show various oscillations. After several numerical experiments with and without the wind input, it was found that the oscillations of the sea level and the oscillations of the depth of the thermocline are caused mainly by the wind, especially when the thermocline depth was not in equilibrium with the prescribed wind system. The sea-level oscillations caused by wind have been observed at tide gauge stations and demonstrated in several works by Professor Hansen in the application of the single-layer model for computations of storm surges in the North Sea. Consequently, in order to obtain a steady state picture of the sea level and currents with a given steady wind, computations should be done over several tidal cycles. This was not possible within this project due to limitations of funds and time.

The wind effects vary considerably from one place to another over the whole Bight. These changes can be followed in Figures 44 to 46. Starting with Point 5, (Figure 44) and following farther offshore (i.e., Figure 45, Point 7, and Figure 46, Point 10) it can be observed that the fluctuations of the mixed layer depth increase with increasing depth and

increasing distance from the coast, whereas the sea-level change (amplitude of the tides) decreases as already observed with a single-layer model. These figures also show currents in both layers at two-hourly intervals, showing that the currents in the second layer turn more to the opposite direction of surface currents with increasing distance from the coast, thus compensating the transport in the surface layer.

At Point 20 (Figure 47), the crest of the mixed layer depth occurs approximately midway between high and low water at the surface (i.e., about 4 to 5 hours before the change at the surface). This is a theoretically correct case for progressive waves. Considerable variation occurred from this case, however, as Figures 45 and 46 indicate.

3.2 CURRENTS IN TWO LAYERS

Comparisons of the speed and direction of mean tidal currents at Ambrose Channel Lightship with the tidal currents in the surface layer as computed with the two-layer HN model using a wind of 9 m sec^{-1} from the SW are shown in Figure 48. The computed currents show somewhat stronger outflow from the Lower Bay, which might be partly due to the fact that the East River was programmed wider in this model than in the nature, thus allowing greater flow from Long Island Sound.

The effects of SW winds on the surface layer currents are apparent in Figures 49 and 50 where the current data extracted from various output points are presented as examples. An inter-comparison of currents in Figures 51 to 57 and the locations of corresponding points (Figure 1) shows the various effects of distance from the coast and water depth on the currents in both layers. Especially noticeable and of practical importance is the shoreward movement of currents in the lower layer off Long Island (Figures 53 to 55).

The shoreward movement of bottom drifters has been observed in this area as well as in Hudson Submarine Canyon by Horne (1971), NOAA (1972) and Callaway (MS) which verifies the correctness of the two-layer HN model in reproducing the currents and suggests that the area off Long Island is unsuitable for the disposal of large amounts of sludge.

A comparison of the strength of the currents in upper and lower layers presented in Figures 49 to 57 reveals that the currents are of about the same strength at both depths. This condition was found by Haight (1942) from direct current measurements. Only in Hudson Submarine Canyon (and possibly in the Ambrose Channel) does the current in the lower layer have a higher velocity during flood than in the surface layer. It should be emphasized, however, that the directions of net flow in the surface and lower layers can be considerably different, and that these differences vary with locations and winds.

Figures 58 to 65 give snapshot pictures of the horizontal currents in the upper and lower layers during various stages of the tide with reference to the Sandy Hook tides. Of considerable interest in these figures are two conditions: First, the effect of the Hudson Submarine Canyon can be traced clearly in every figure (see bathymetry of the Bight in Figure 69). There is a greater in- and outflow along the axis of the canyon and sometimes a gyral is located at its mouth on the continental slope. Secondly, most of the water flowing into the New York Bight along the canyon is flowing to the south off Atlantic City. The effects of wind are also clearly recognizable on these figures, especially in areas where they are not masked by other strong currents (i.e., off Long Island). A comparison of upper and lower level currents at the same output time indicates considerable differences of net current direction and some differences in speed in both layers.

3.3 TRANSPORT AND DISPERSION OF POLLUTANTS

The transport of water and net circulation in a relatively shallow bight (e.g., the New York Bight) is determined greatly by winds as well as tides. Thus for a complete investigation of transport and flushing, computations must be made with various prevailing winds. The computed data on transport through various sections are available in computer printouts and only a few examples are presented below.

The transport rates through section BB6 (location, see Figure 1) in the upper layer in calm conditions and with 9 m sec^{-1} winds from SW are shown in Figure 66. Although the transport varies in both cases in tidal rythm, the eastward component prevails with the SW winds. The net transport through the same section is given in Figure 67. In calm conditions a slight westward transport occurs through section BB6 which is in agreement with the general circulation pattern in the New York Bight. With SW winds the net transport through this section is toward the east.

Figure 68 shows the computed concentration of "pollutants" in the upper layer 24 hours after instantaneous release. The same limitations of diffusion computations apply to the relatively coarse two-layer model as to the single-layer, large grid size model. The results shown in this figure are also similar to the corresponding results from the single-layer model. Thus in order to compute dispersion and diffusion with a Lagrangian method in a grid which is larger than half of the distance of tidal excursion, either of the following methods should be used:

a. the excursion of the water particle (e.g., at the center of the release point) can be computed with the HN model as described in Chapter 2.5. The eddy diffusion of the blob can be computed with any Eulerian type of method of which there are several available;

b. the diffusion and dispersion can also be computed with a Lagrangian method in a smaller subgrid, for which the currents are extracted and interpolated in each time step from the large-scale grid output. This method requires an additional computer run.

c. if the diffusing blob is large and initially covers many grid points, dispersion and diffusion computations can be made in a large grid with Lagrangian approach (e.g., distribution of river outflow).

4. RECOMMENDATIONS FOR APPLICATIONS OF THE MODEL RESULTS AND FOR FURTHER DEVELOPMENT

1. As a considerable amount of numerical output (results) is produced by an HN model, it is impossible to describe and reproduce all the possible results in reports. The latter serve mainly to present examples and the model capabilities as well as verifications. In any specific application, and in search for an answer to a specific question, the numerical data in the printouts from the model run should be consulted and/or used.

2. The HN models have proven to be of great use for obtaining data on currents at various levels and with various winds for the computation of diffusion, dispersion and flushing, for selection of proper waste disposal areas, and for a variety of other purposes.

3. Although general verifications of the HN models have been made in various areas, there is a continued need for further specific verification, especially of the multi-layer models. This verification should be done with specific short-term recordings (few days) of (a) sea level at specific points with portable tide gauges, (b) current recordings, and (C) thermal structure variation recordings. (The latter is especially required to improve the boundary input into the multi-layer models.)

4. Additional research is required on the treatment of multiple open boundaries and especially on the methods of input of tides in deeper layers at the open boundaries.

5. The diffusion and dispersion computations require further verification for which results from better large-scale dye experiments can be used (e.g., the multi-national experiments carried out by the International Council for the Exploration of the Sea). Further numerical experimentation is required on the computation of dispersion and diffusion in large grid size models.

6. The single layer HN model has become a proven tool for investigation and reproduction of dynamic processes in shallow coastal waters and estuaries. It would be desirable to use this model for the computation of a number of "type conditions," such as (a) the effects of offshore bars on exchange of coastal waters with offshore waters, (b) the effects of bathymetric slopes and irregularities on currents and mixing, and (c) other conditions pertinent to waste disposal in coastal waters.

REFERENCES

Baumgartner, D.J., 1972: A brief outline of a study of sewage sludge dumping in the New York Bight. Mimegr. Rpt. EPA, Pac. NW Env. Res. Lab.

Callaway, R., MS: Bottom drifter study in New York Bight.

Haight, F.J., 1942: Coastal currents along the Atlantic Coast of the United States. U.S. Dept. of Commerce, Coast and Geodetic Survey, Spec. Publ. 230: 73 pp.

Horne, R.A., A.J. Mahler and R.C. Rossello, 1971: The marine disposal of sewage sludge and dredge spoil in the waters of the New York Bight. Woods Hole Oe. Inst., MS rpt to coastal Eng. Res. Center, Corps of Engineers.

Ketchum, B.H., A.C. Redfield and J.C. Ayers, 1951: The oceanography of the New York Bight. Papers in Phys. Oceanogr. and Met. Cambridge and Woods Hole, 12(1): 1-46.

McClennen, C.E., 1973: New Jersey continental shelf near bottom current meter records and recent sediment activity. J. Sedimentary Petrology, 43(2):371-380.

NOAA, 1972: The effects of waste disposal in the New York Bight. Sect. 6. Surface and bottom water movement. Rpt. for Coastal Eng. Res. Center., Corps of Engineers.

Pearce, J.B., 1970: The effects of waste disposal in the New York Bight - Interim Rpt. for Jan 1970. MS Rpt for Corps of Engineers.

Powers, C.F. and J.C. Ayers, 1951: Drift bottle studies in the Newport Bight and New York Bight areas. MS rpt to ONR (N6 onr 264, task 15).

Reports in this series:

Part 1: A vertically integrated hydrodynamical-numerical model (W. Hansen type): Model description and operating/running instructions.

Part 2: A multi-layer hydrodynamical-numerical model (W. Hansen type): Model description and operating/running instructions.

Part 3: Computation of tides, currents and dispersal of pollutants in Lower Bay and Approaches to New York with fine and medium grid size hydrodynamical-numerical models.

Part 4: Computation of tides, currents, and dispersal of pollutants in the New York Bight from Block Island to Atlantic City with large grid size, single and two-layer hydrodynamical-numerical models. (This report.)

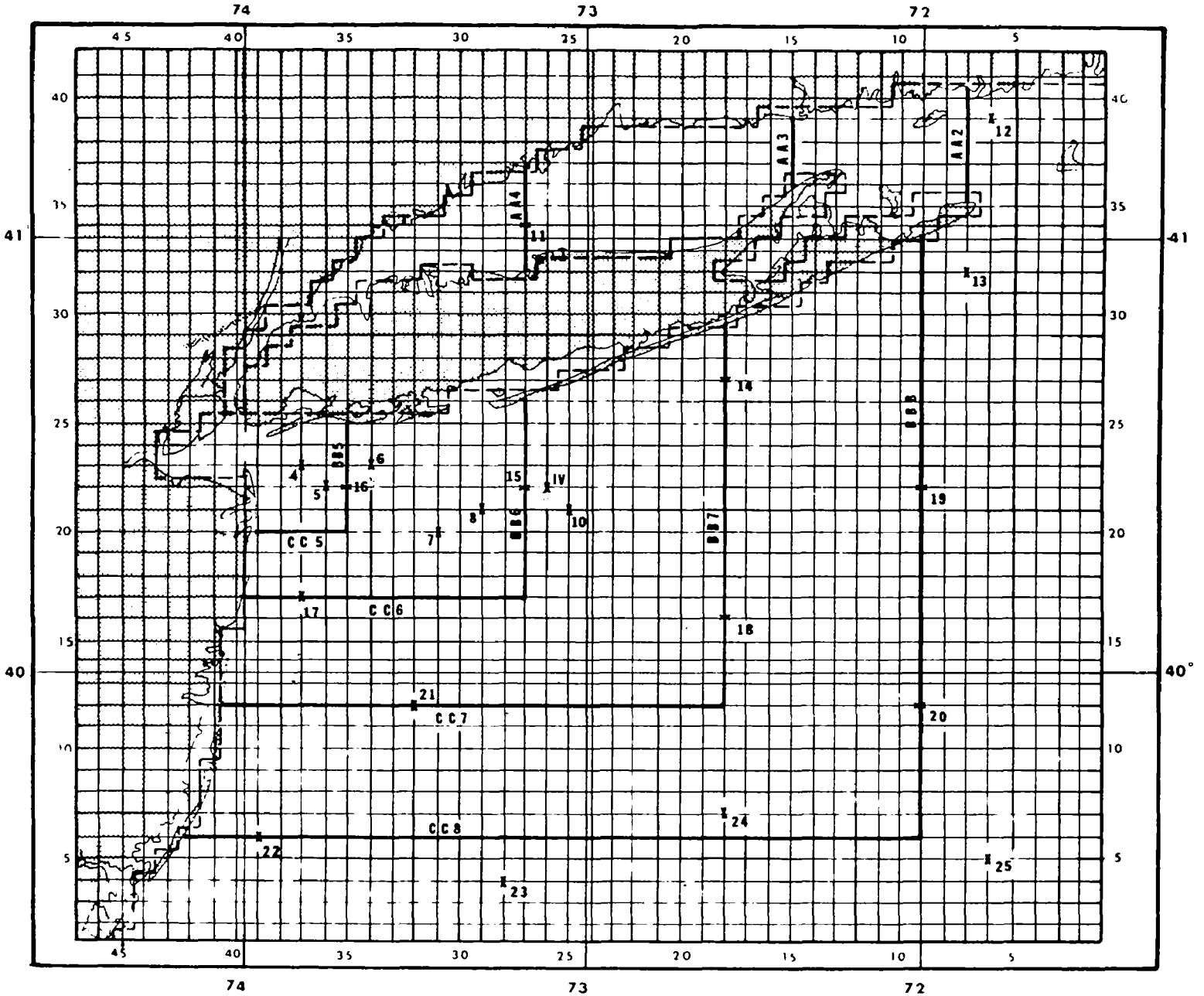

Figure 1 Computational grid and locations of special output points and sections in the single layer model

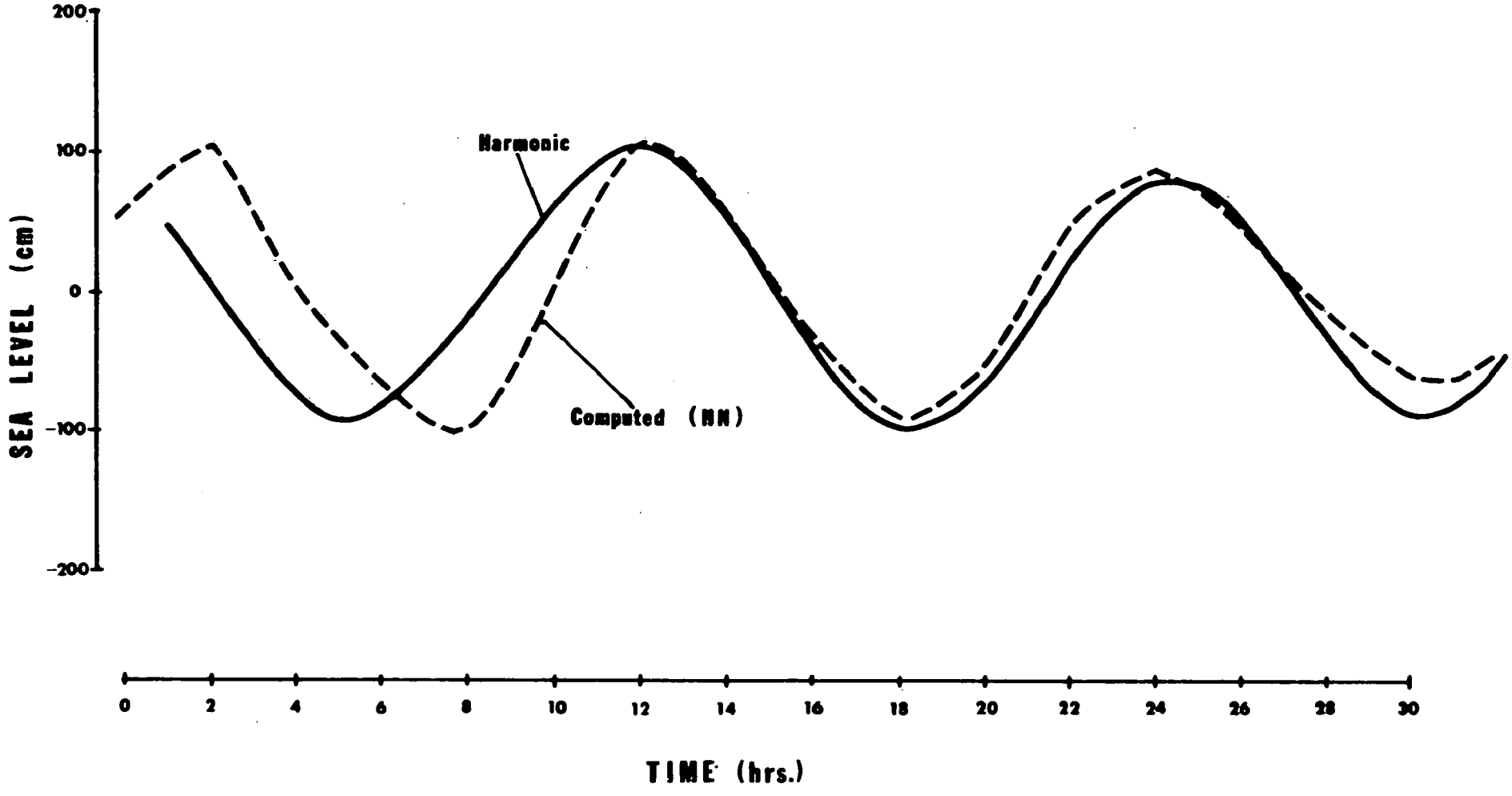

Figure 2 Tides at Sandy Hook, computed with harmonic method and with HN model

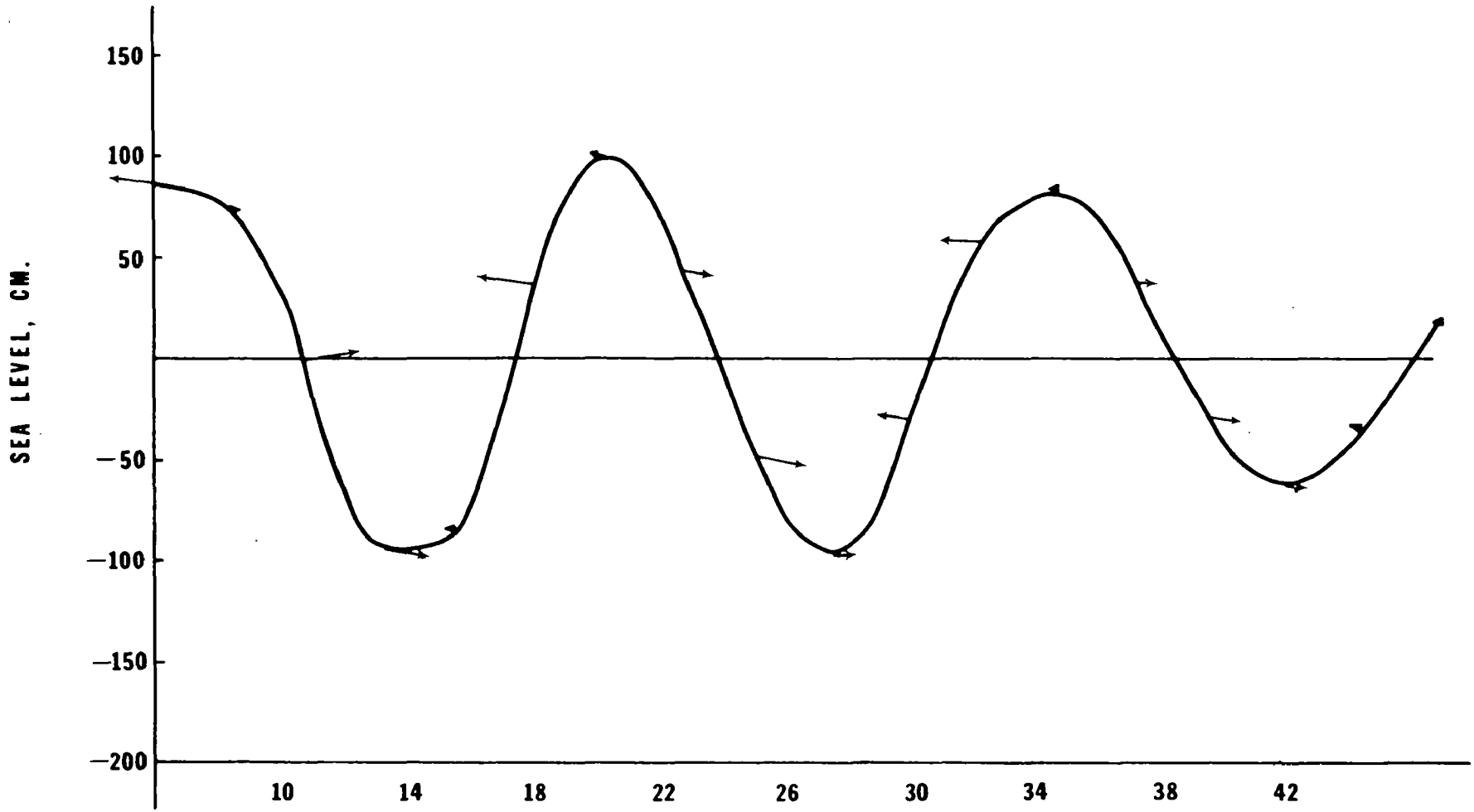

Figure 3 Sea level change and currents at Point 5 (location see Figure 1)

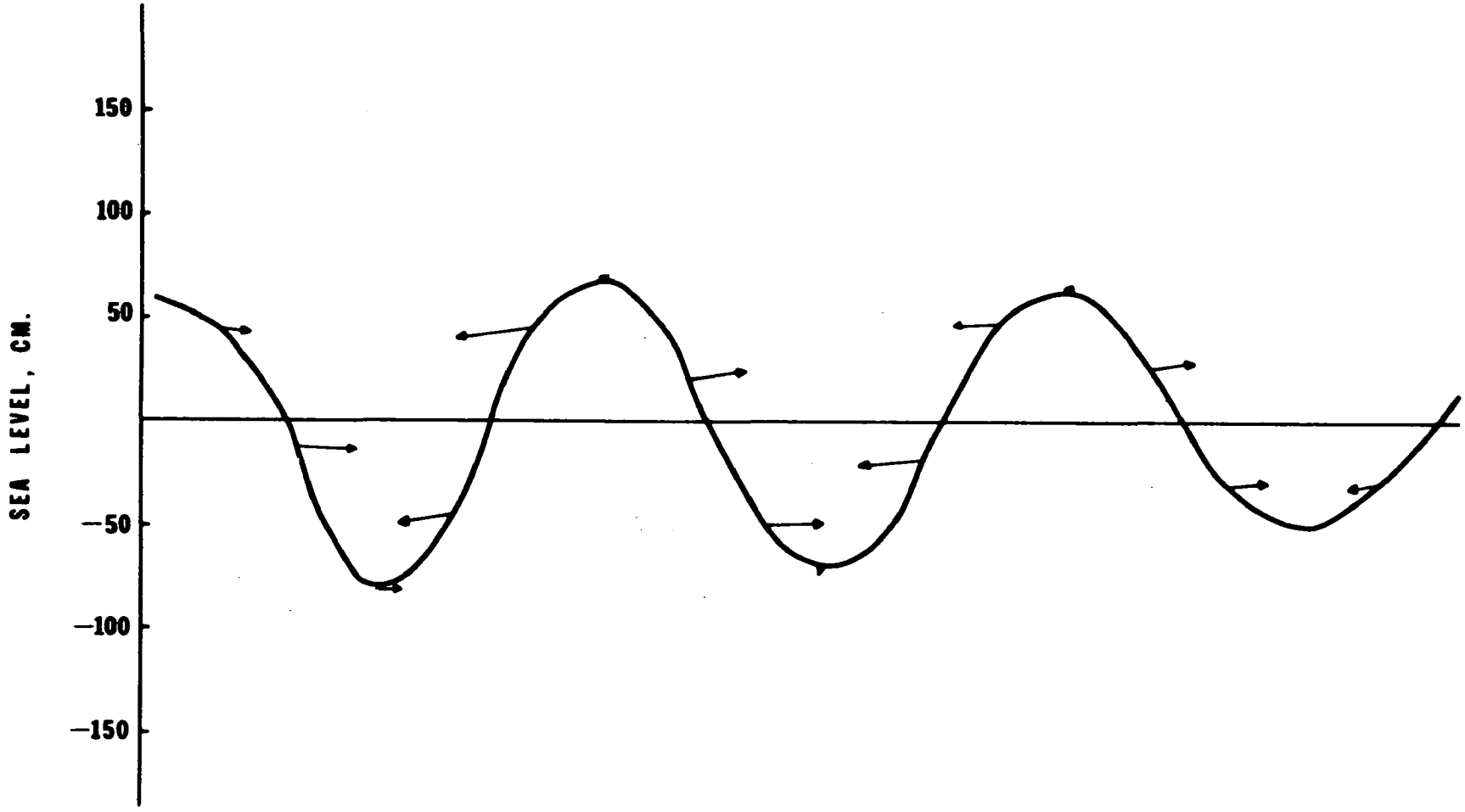

Figure 4 Sea level change and currents at Point 10 (location see Figure 1)

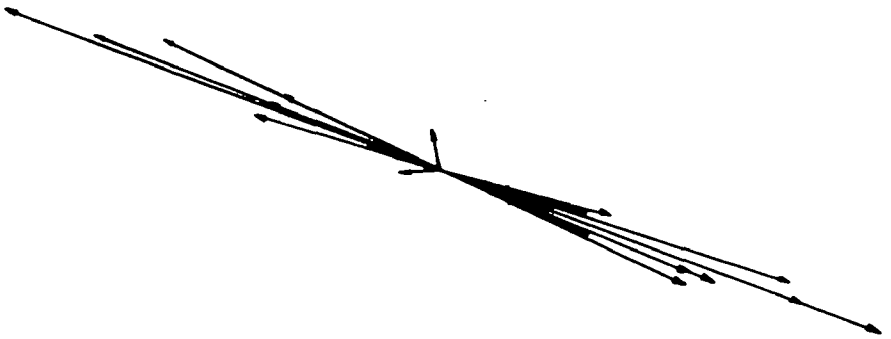

Figure 5 Computed currents at Point 4 (locations see Figure 1)

Figure 6 Computed currents at Point 5 (location see Figure 1)

Figure 7 Computed currents at Point 6 (location see Figure 1)

Figure 8 Computed currents at Point 10 (location see Figure 1)

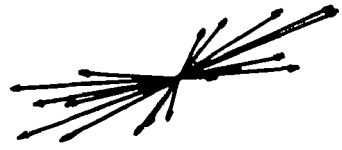

Figure 9 Computed currents at Point 13 (location see Figure 1)

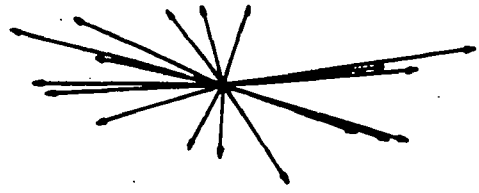

Figure 10 Computed currents at Point 18 (location see Figure 1)

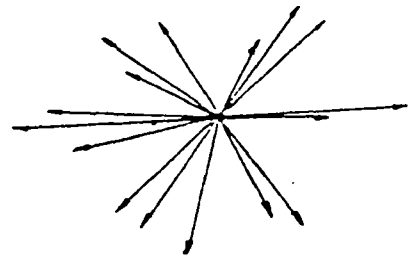

Figure 11 Computed currents at Point 19 (location see Figure 1)

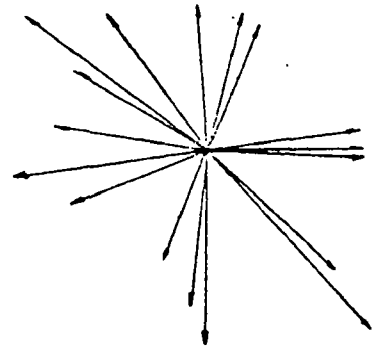

Figure 12 Computed currents at Point 20 (location see Figure 1)

Figure 13 Computed currents at Point 21 (location see Figure 1)

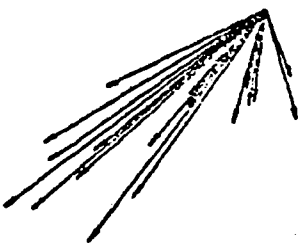

Figure 14 Computed currents at Point 22 (location see Figure 1)

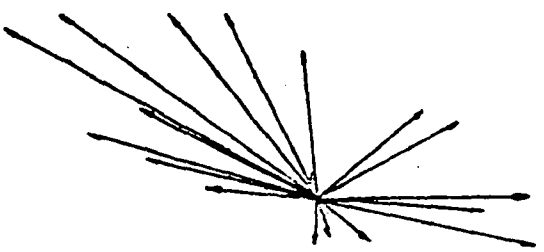

Figure 15 Computed currents at Point 24 (locatior see Figure 1)

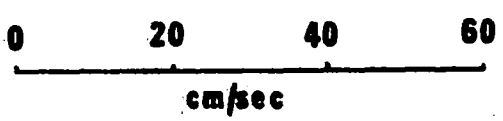

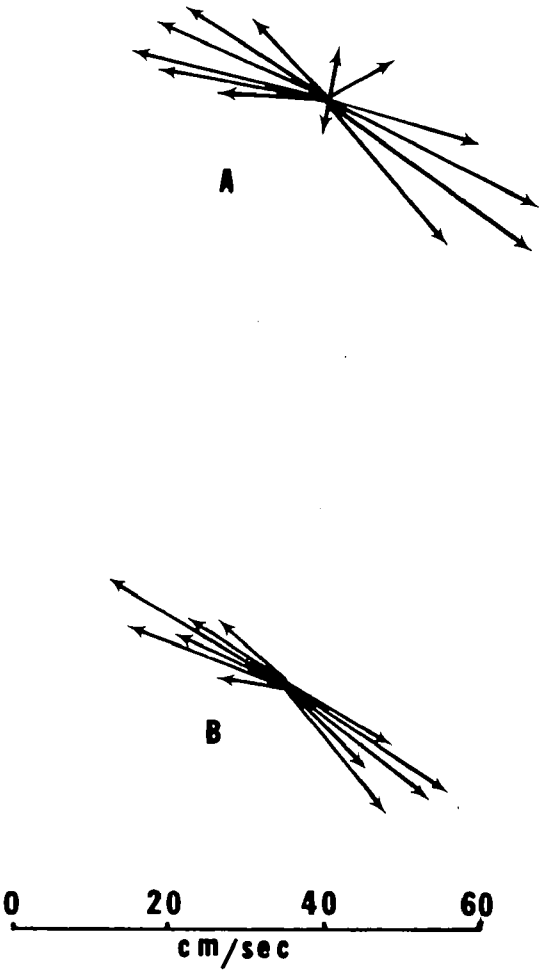

Figure 16 A Mean tidal currents at Scotland Lightship (40°26.6'N; 73°55.2'W) (from Haight, 1942)
B Tidal currents (spring tides) at grid point 22,37 (see Figure 1).

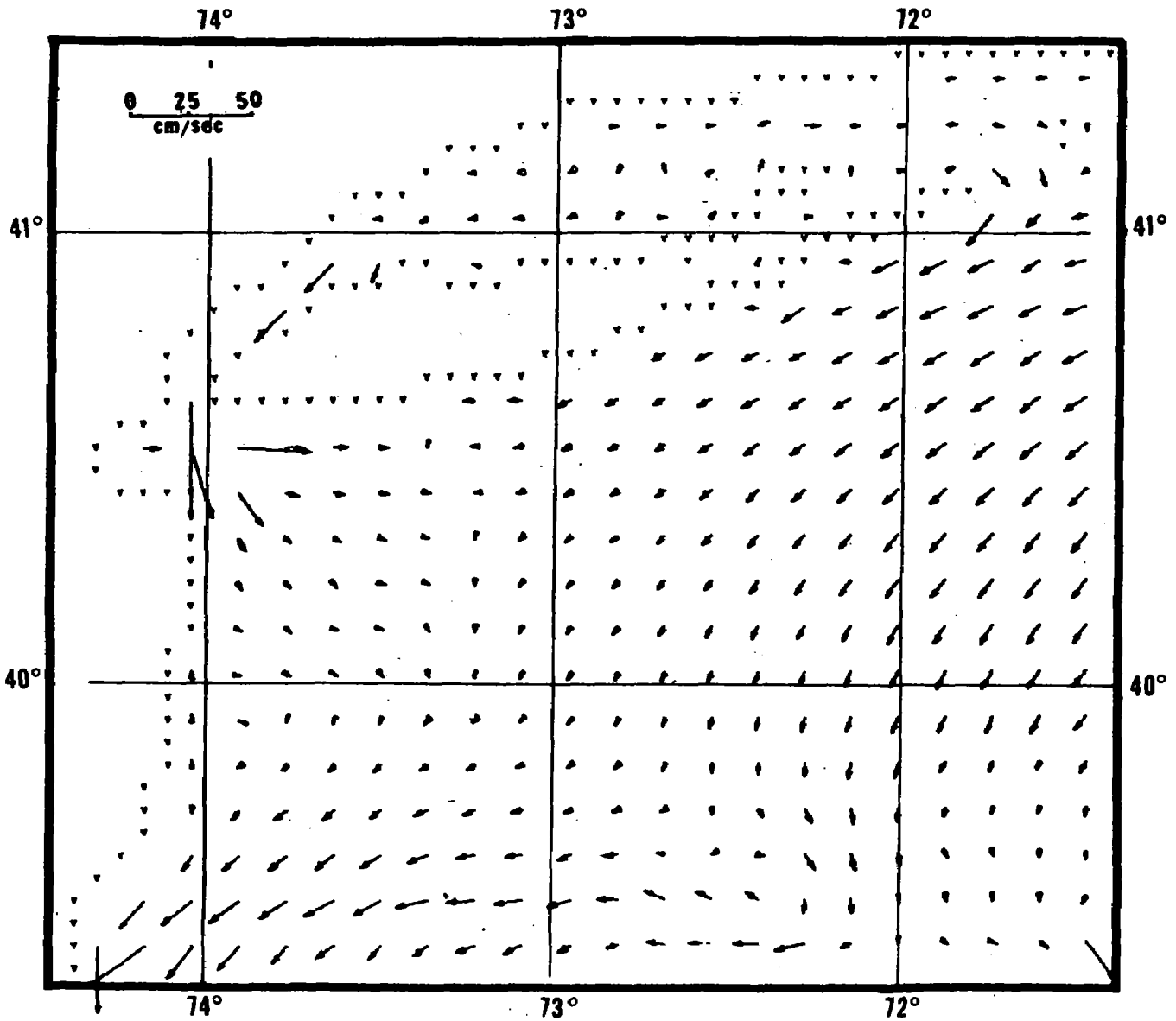

Figure 17 Currents during low water at Sandy Hook

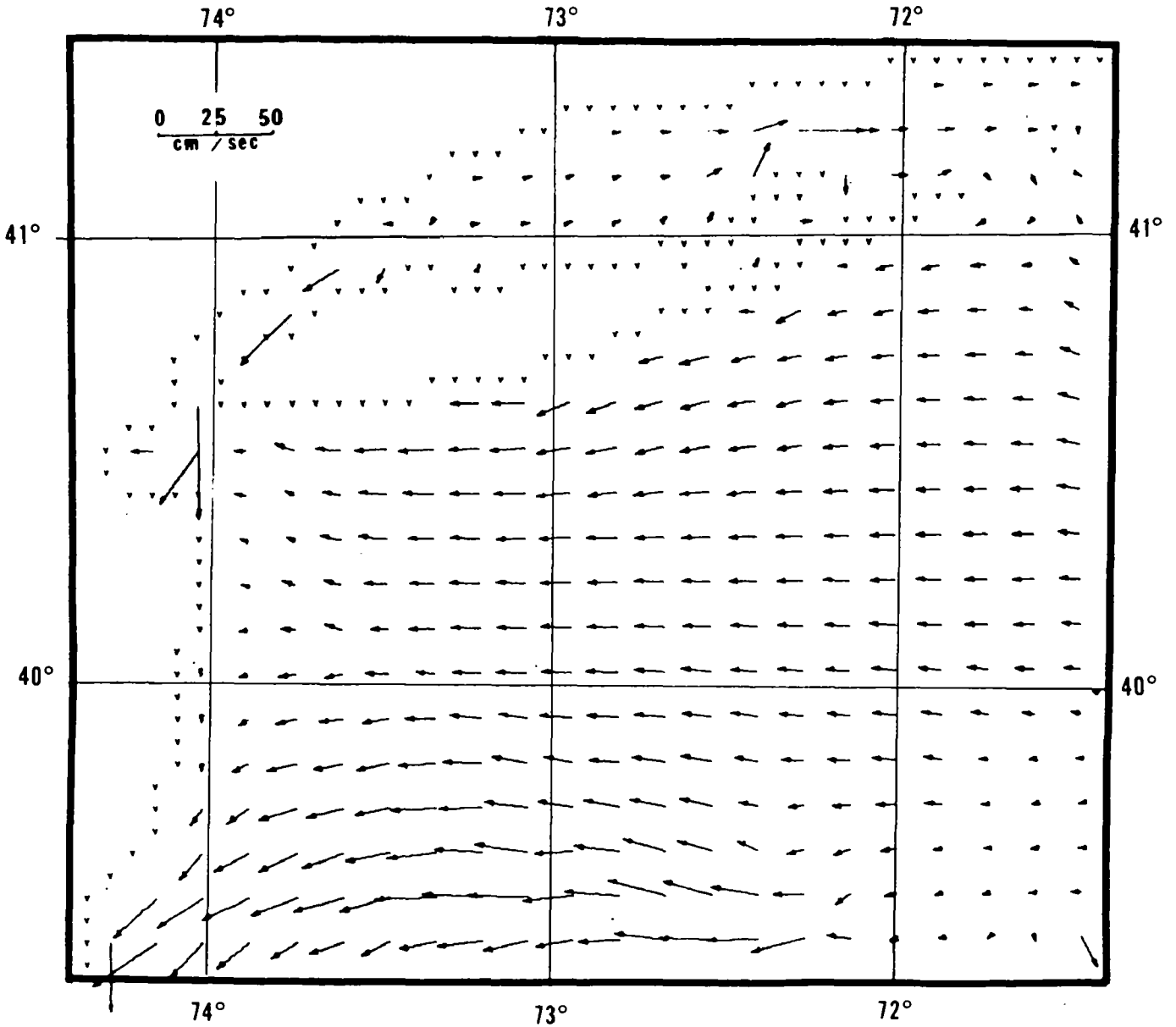

Figure 18 Currents during 2 hours after low water at Sandy Hook

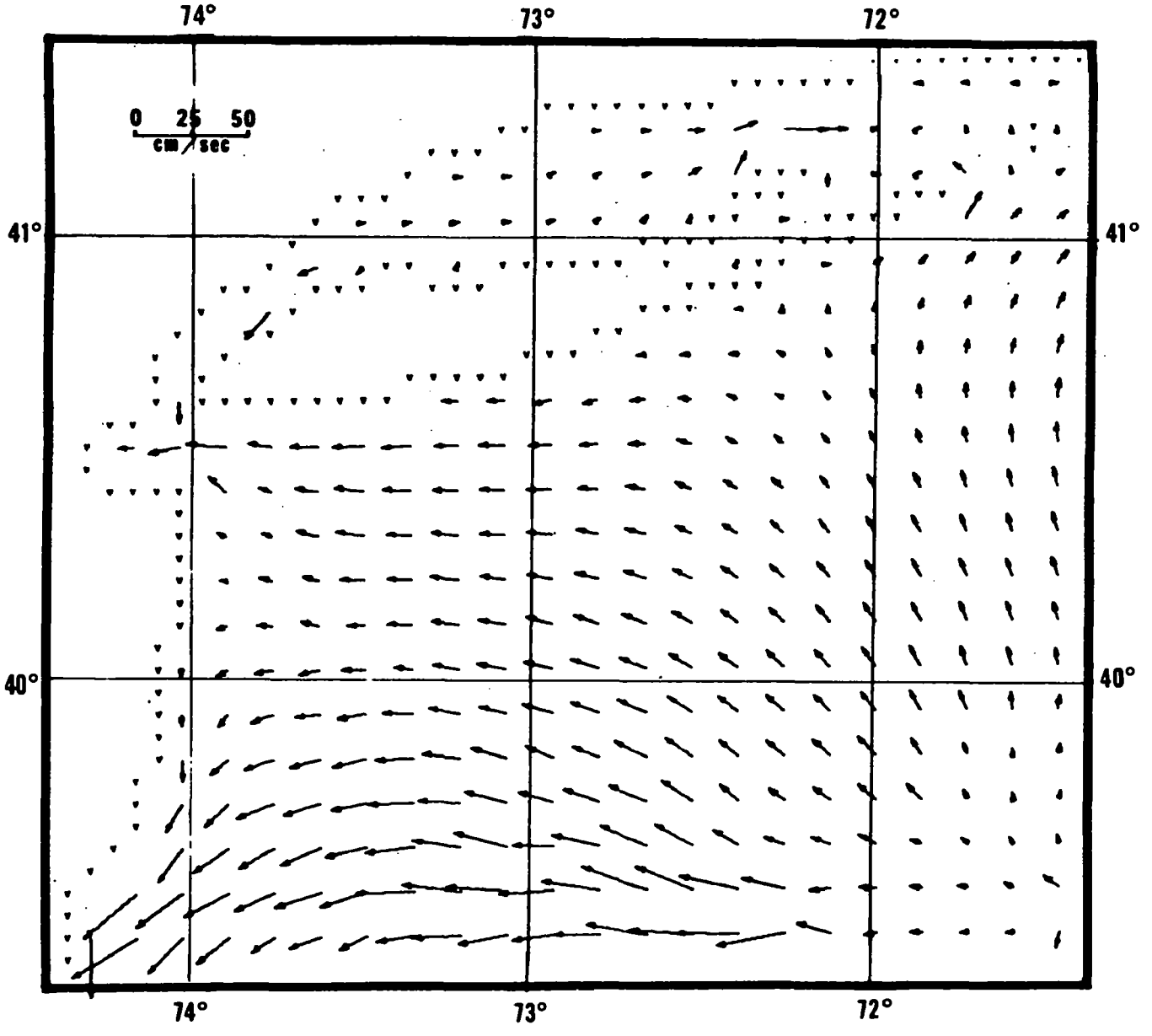

Figure 19 Currents during 2 hours before high water at Sandy Hook

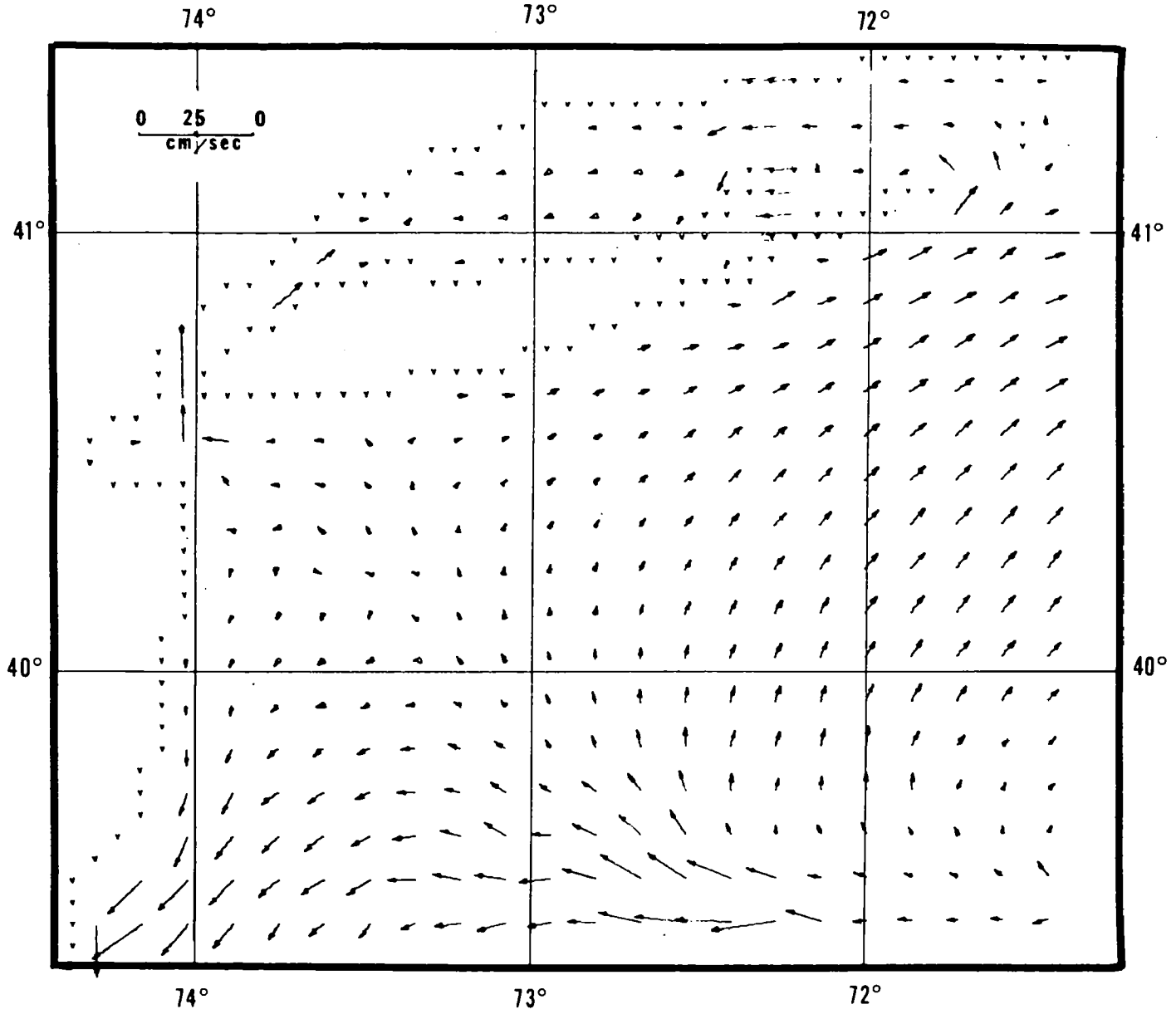

Figure 20 Currents during high water at Sandy Hook

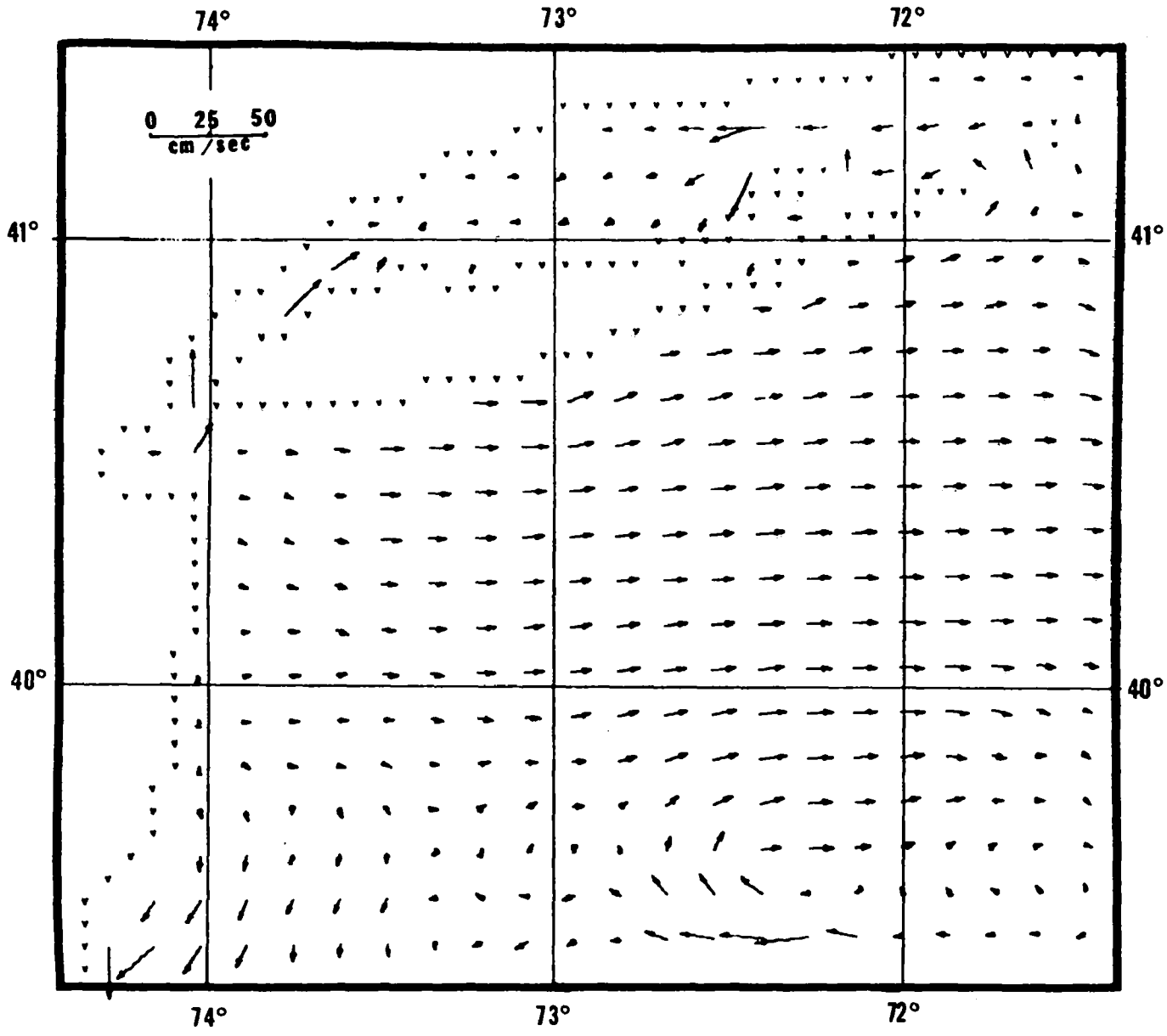

Figure 21 Currents during 2 hours after high water at Sandy Hook

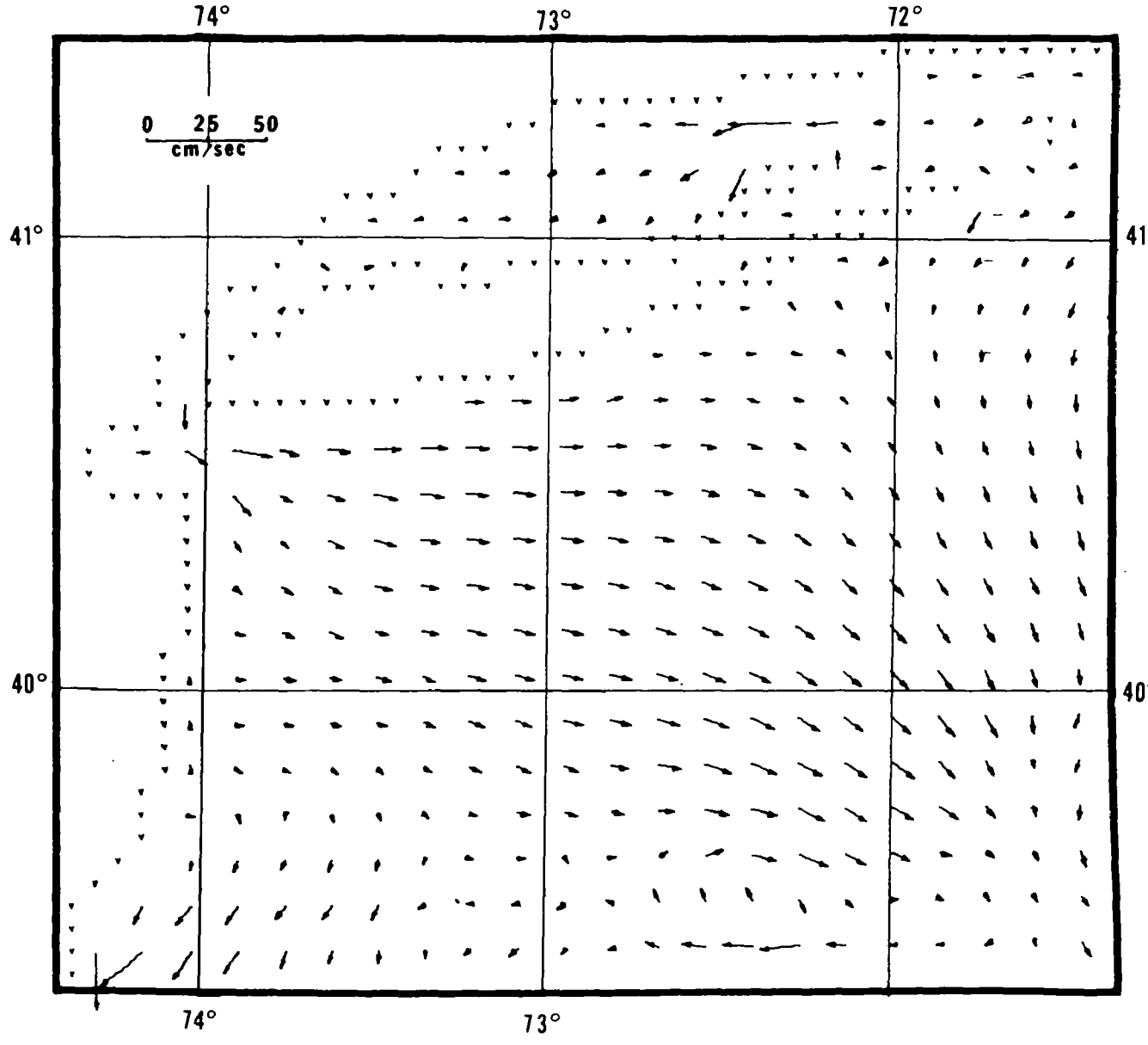

Figure 22 Currents during 2 hours before low water at Sandy Hook

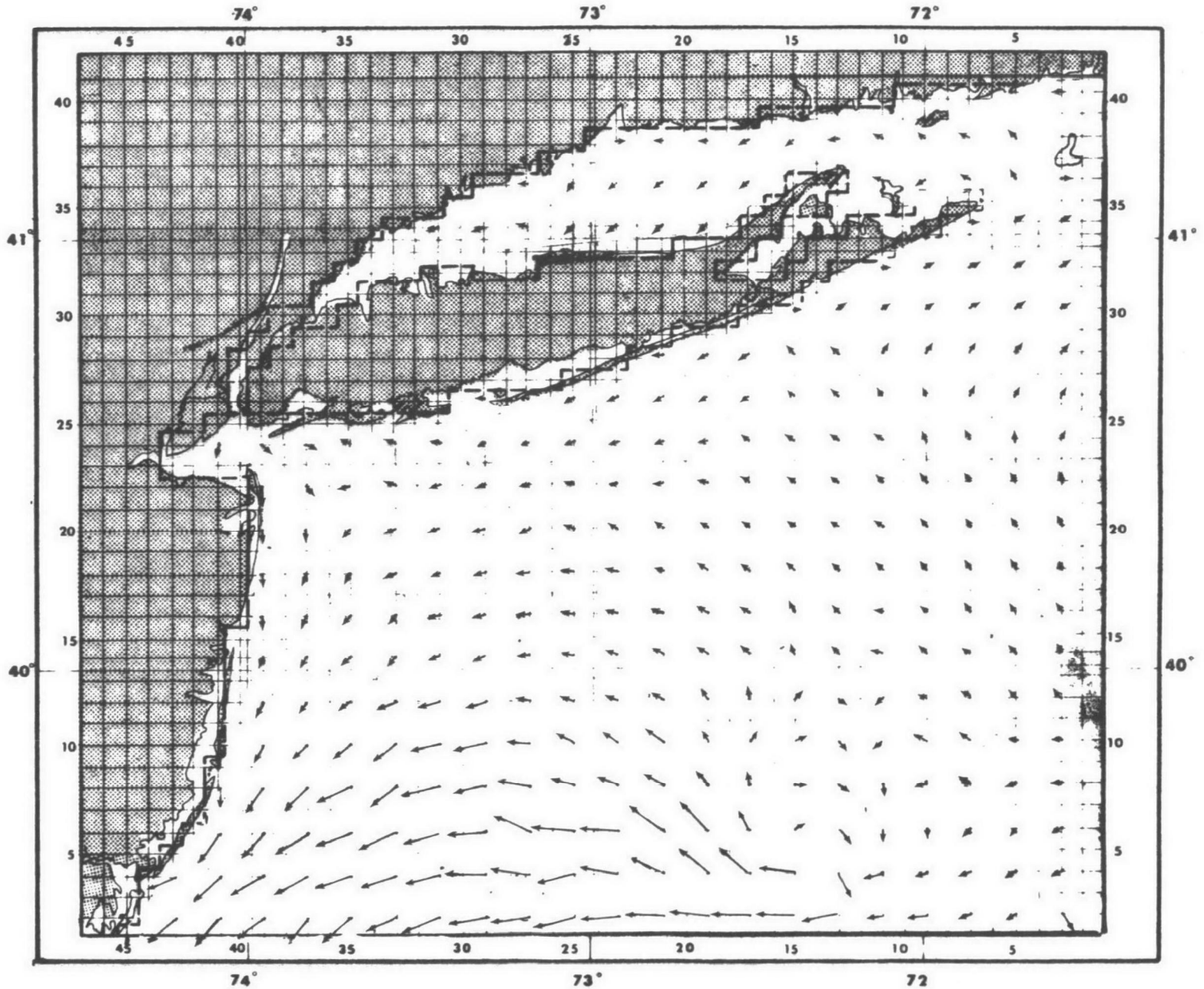

Figure 23 Rest currents after a full tidal cycle and with SW wind, 9m sec^{-1}

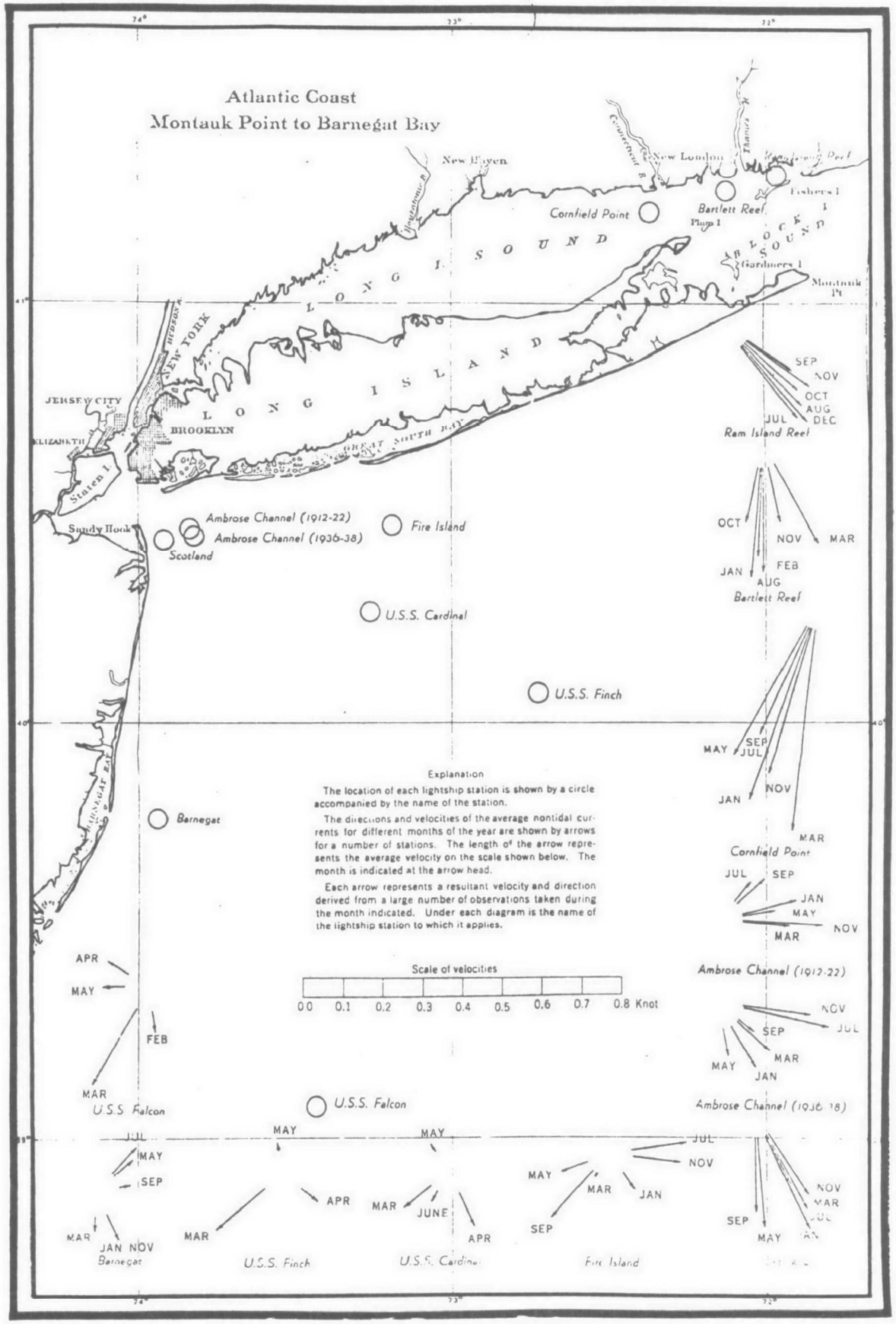

Figure 24 Nontidal currents at Lightship stations, Montauk Point to Barnegat Bay (Haight, 1942)

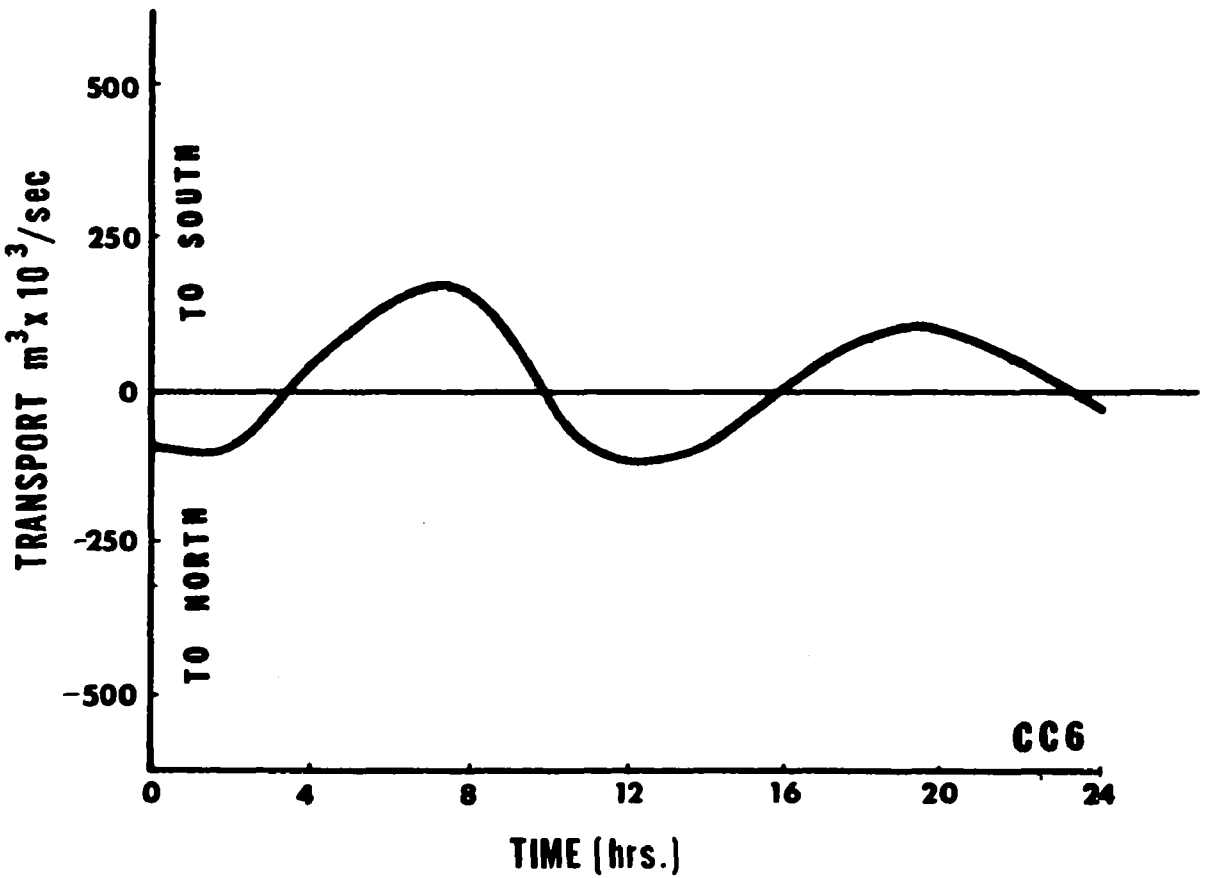

Figure 25 Transport through section CC6

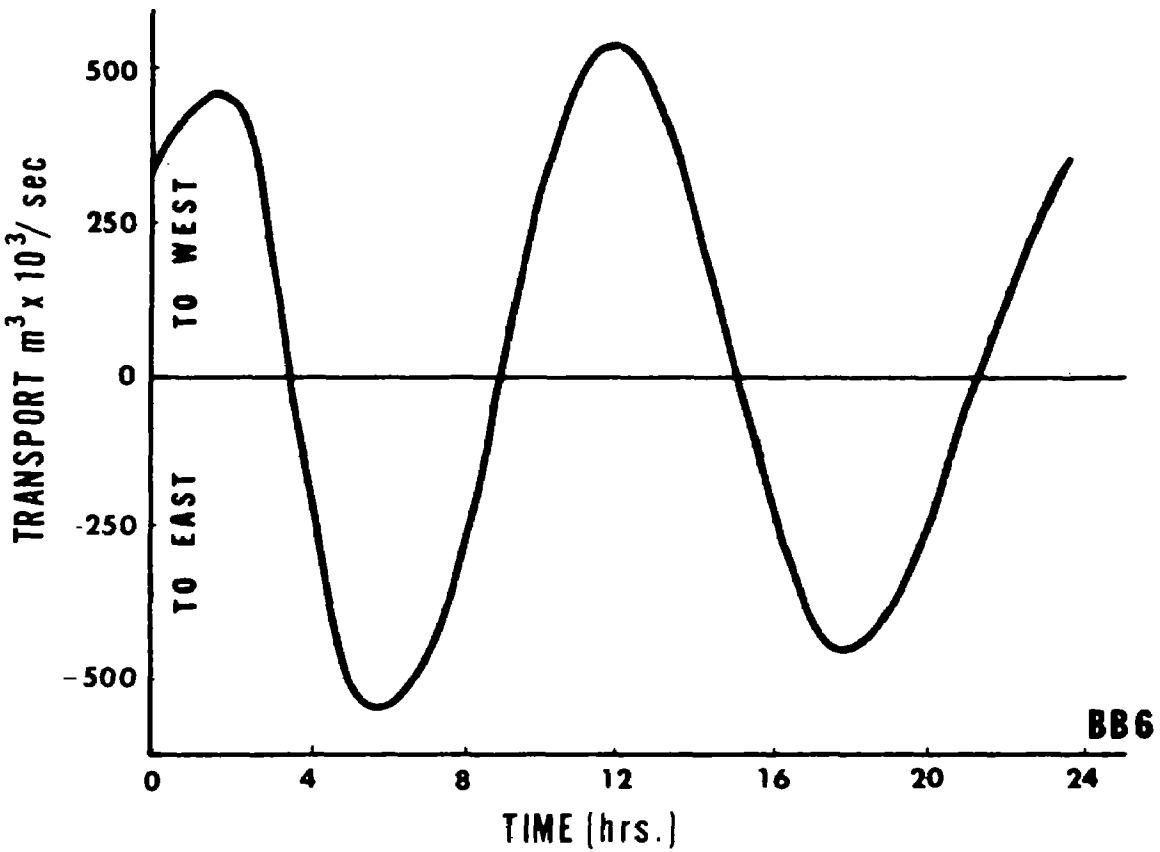

Figure 26 Transport through section BB6

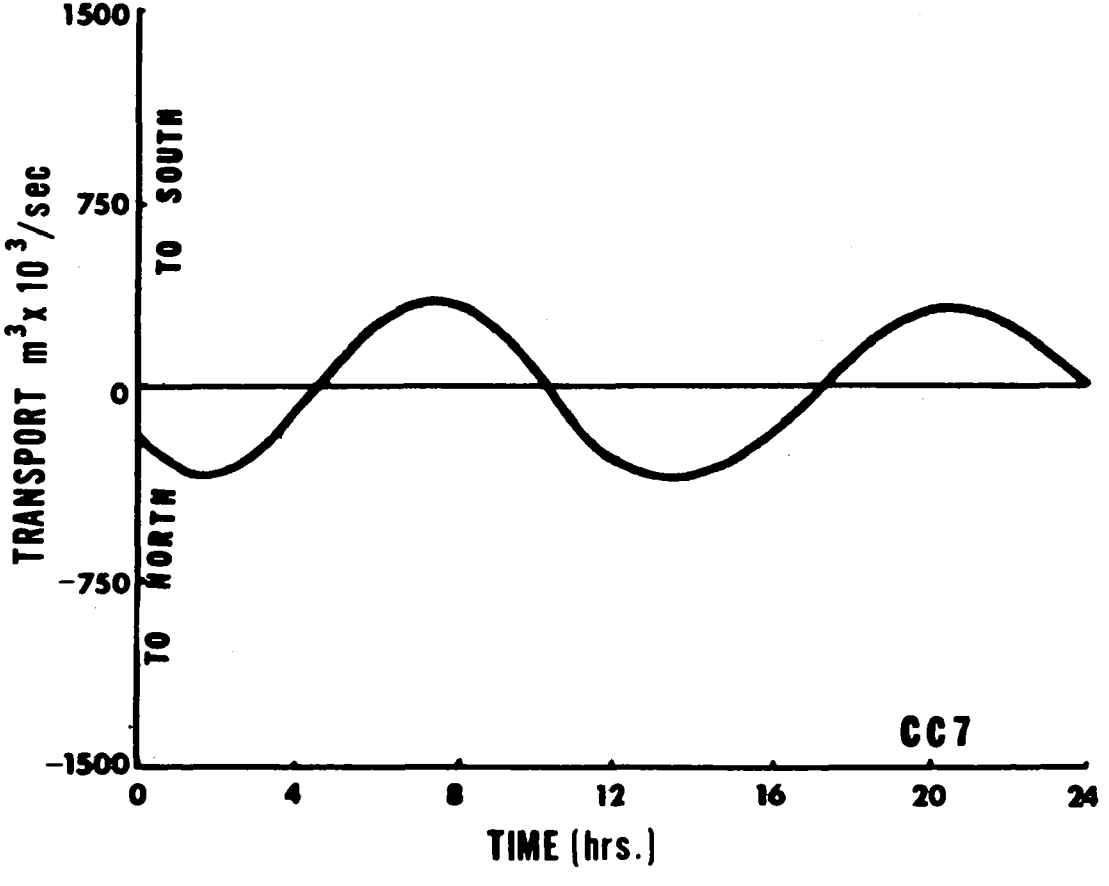

Figure 27 Transport through section CC7

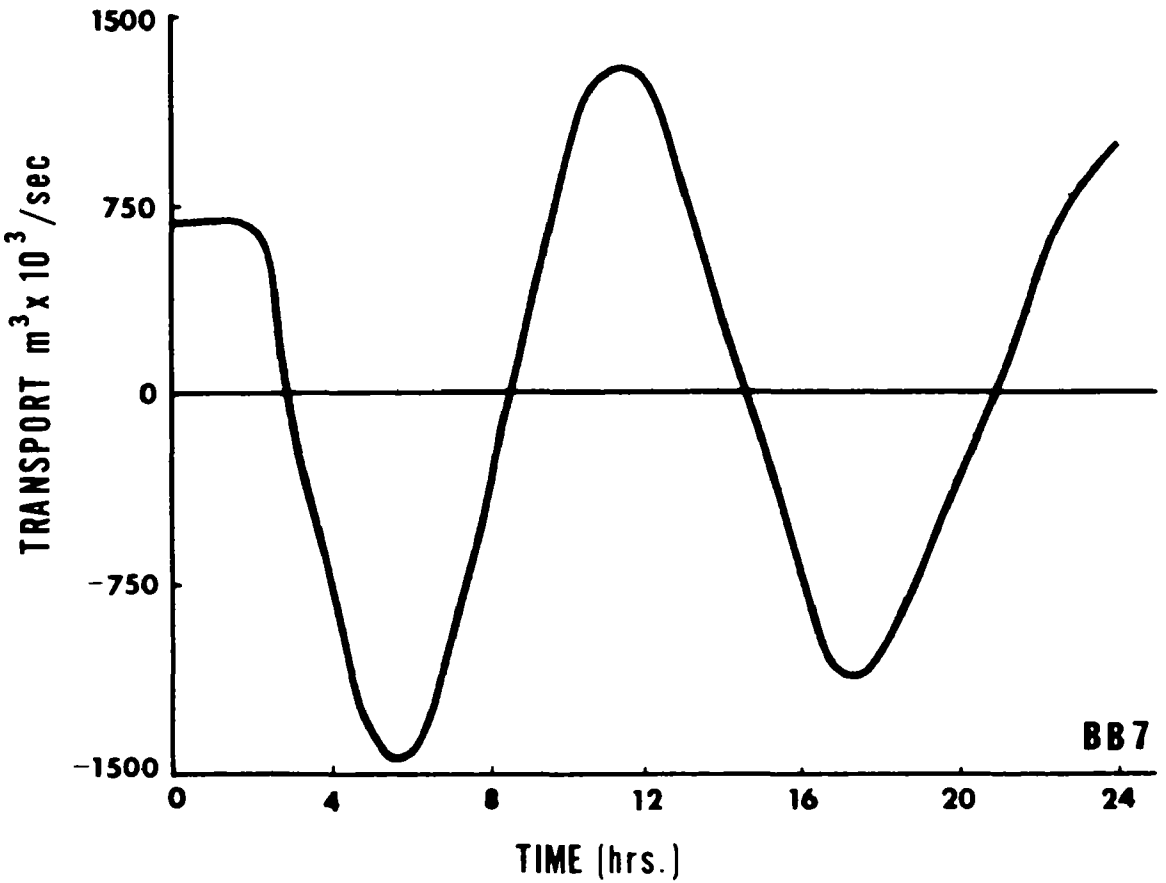

Figure 28 Transport through section BB7

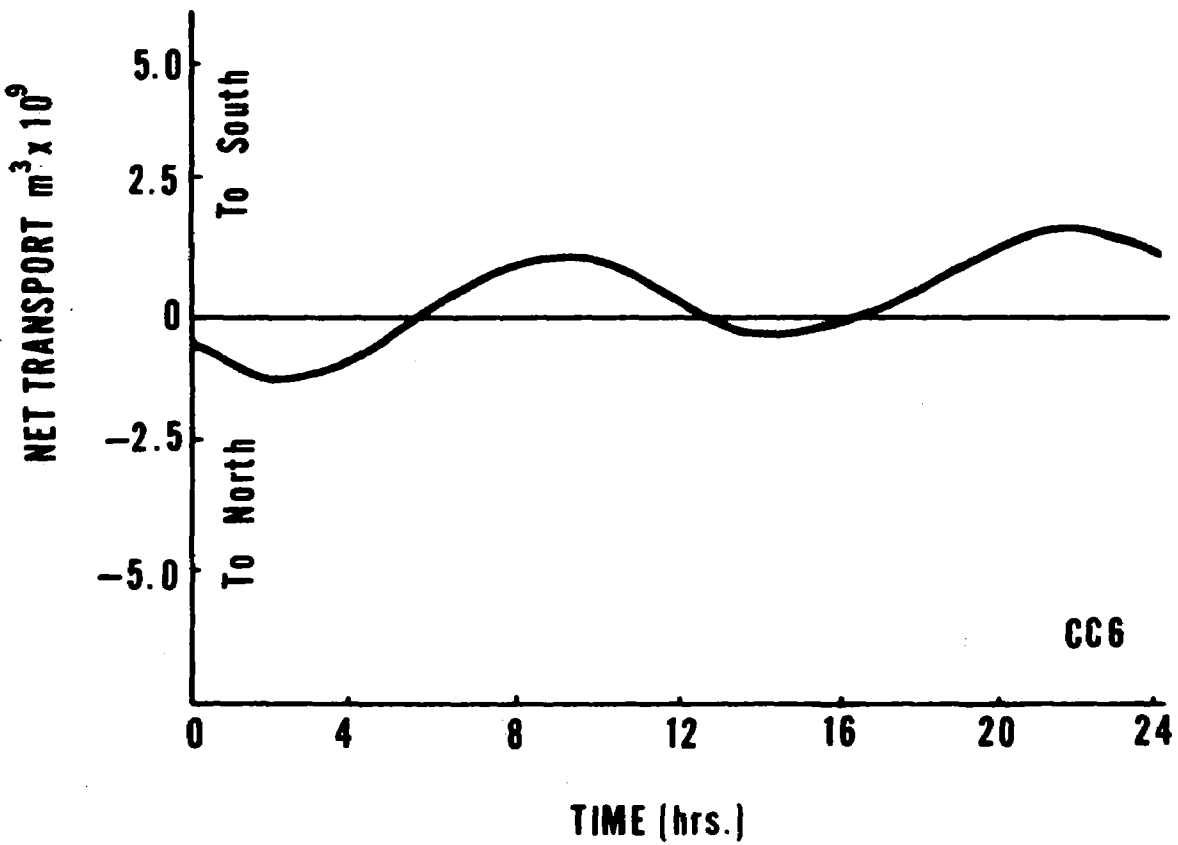

Figure 29 Net transport through section CC6

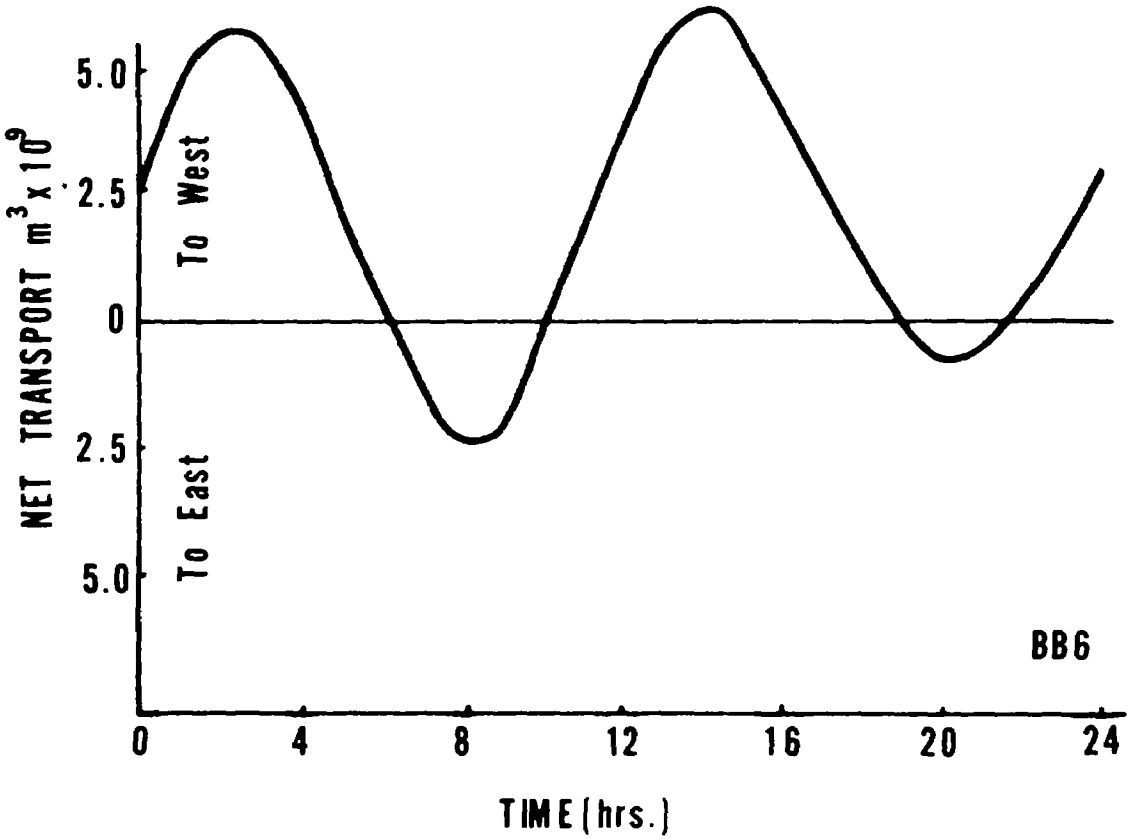

Figure 30 Net transport through section BB6

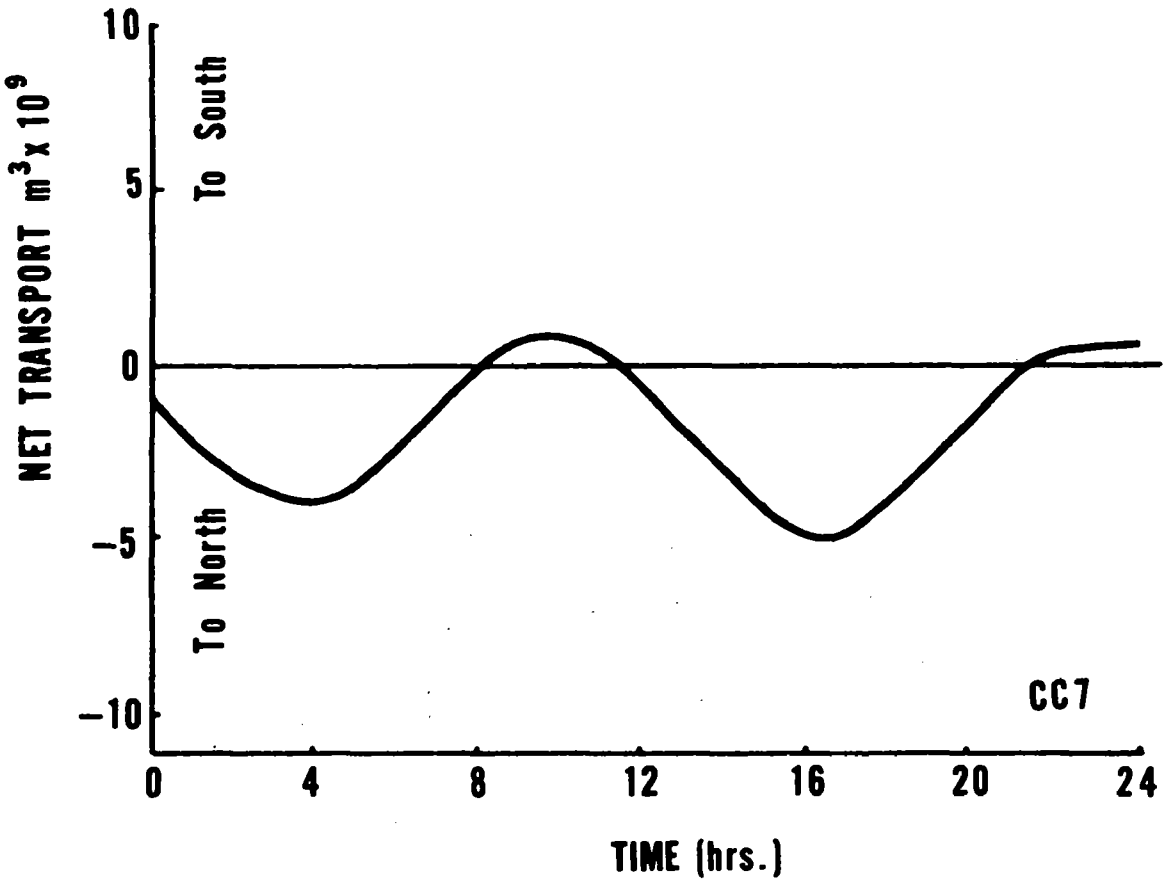

Figure 31 Net transport through section CC7

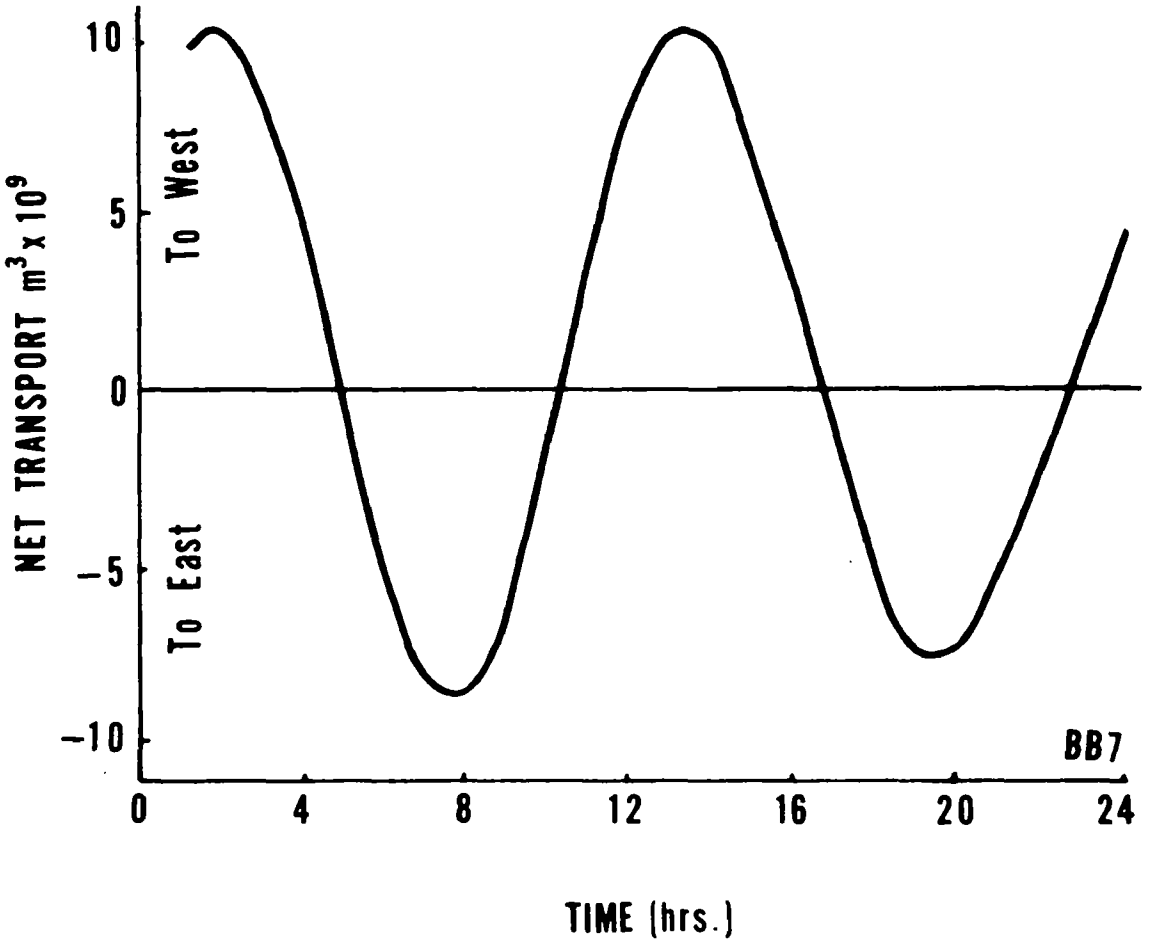

Figure 32 Net transport through section BB7

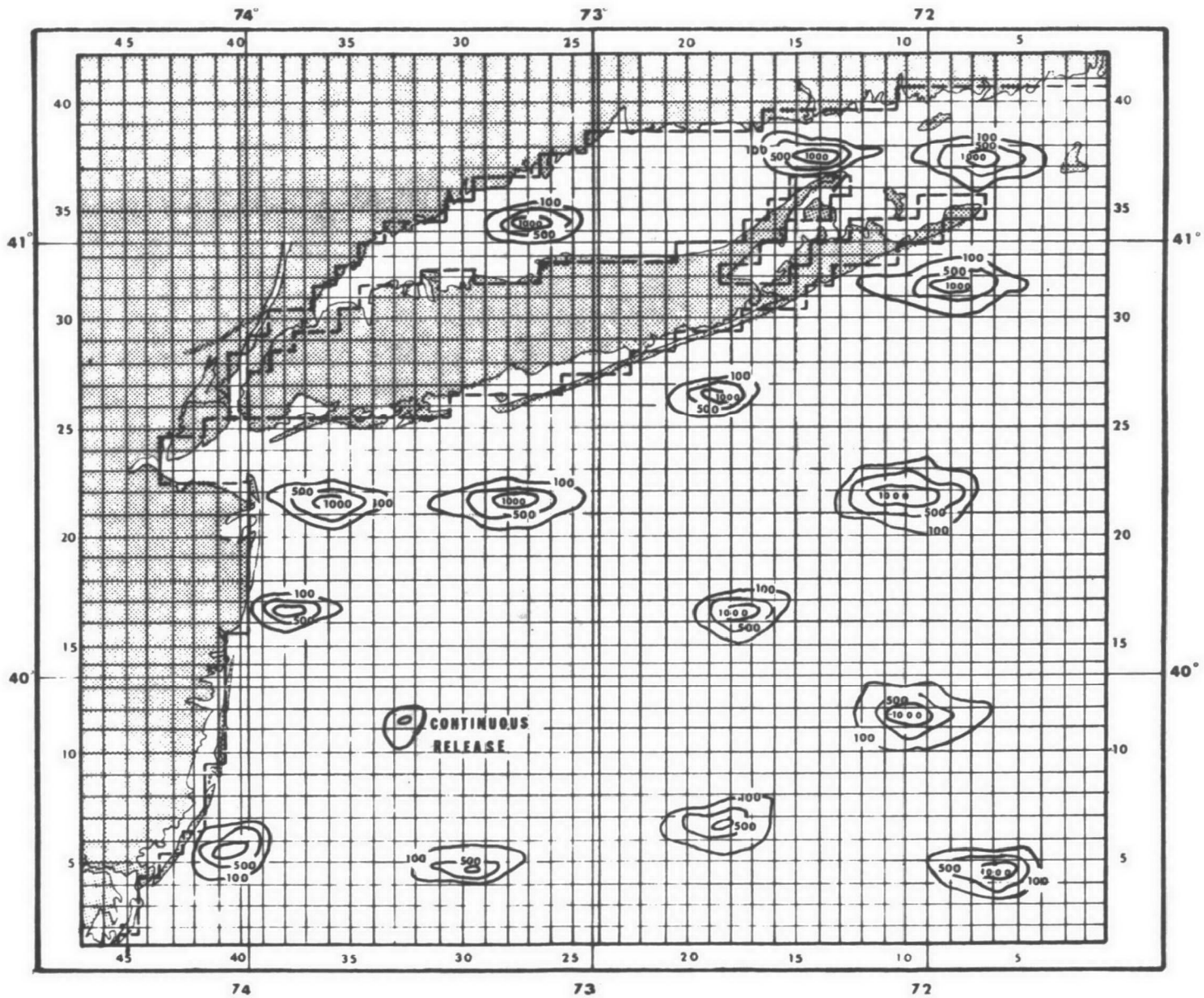

Figure 33 Concentration of "pollutants" after a full tidal cycle (initial release 10000 units each point)

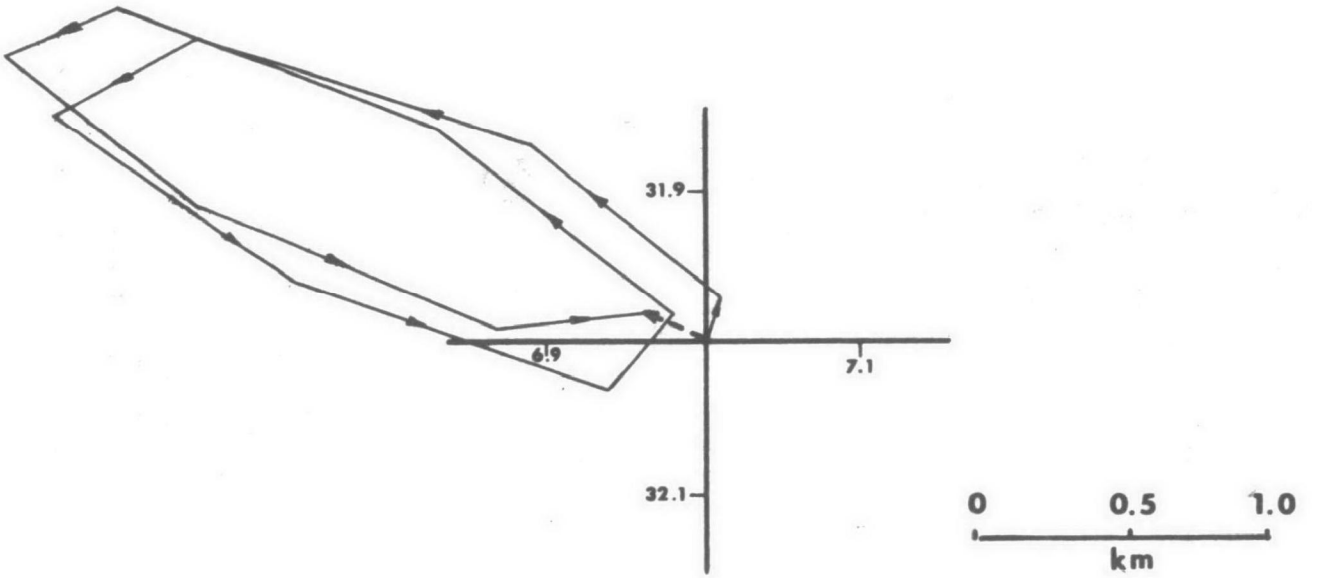

Figure 34 Movement of a water particle during one tidal cycle at Point 13 (location see Figure 1) (Wind 9m/sec, from SW)

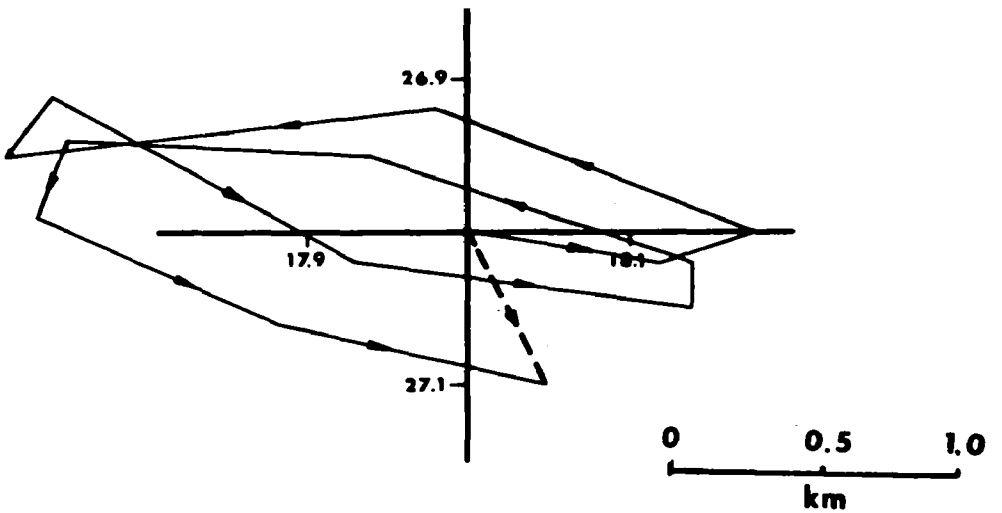

Figure 35 Movement of a water particle during one tidal cycle at Point 14 (location see Figure 1) (Wind 9m/sec, from SW)

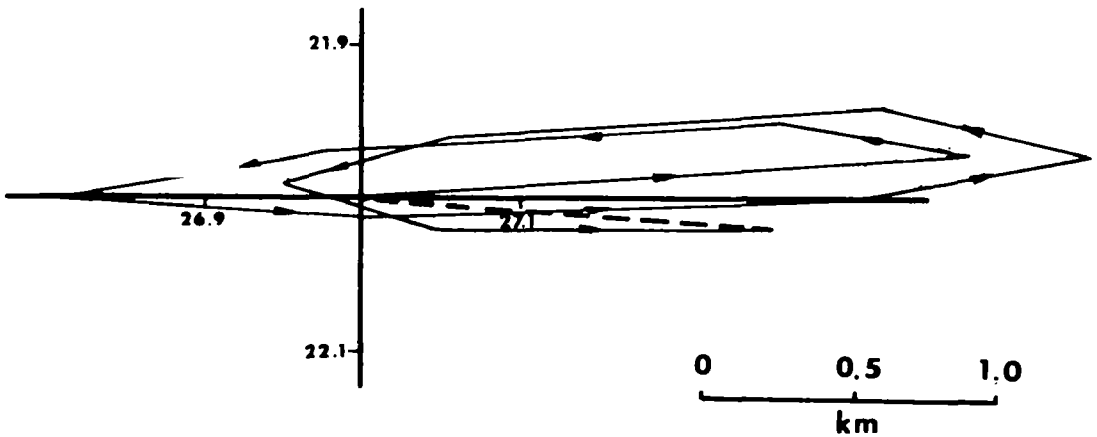

Figure 36 Movement of a water particle during one tidal cycle at Point 15 (location see Figure 1) (Wind 9m/sec, from SW)

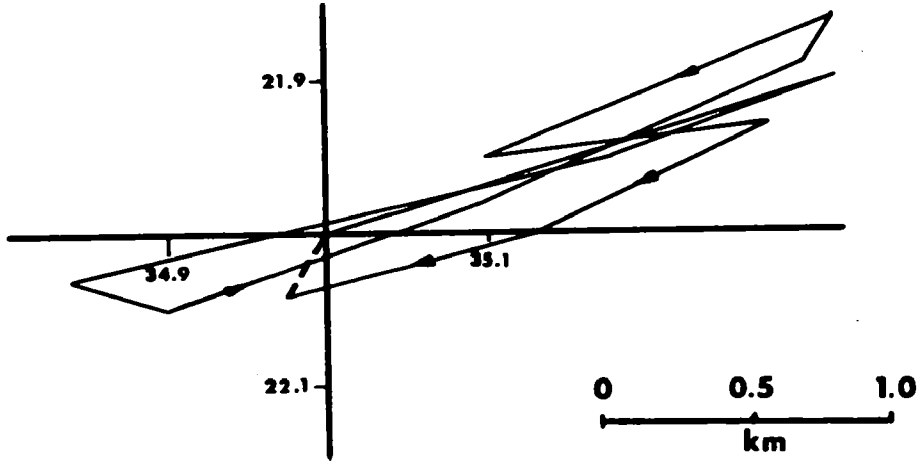

Figure 37 Movement of a water particle during one tidal cycle at Point 16 (location see Figure 1) (Wind 9m/sec, from SW)

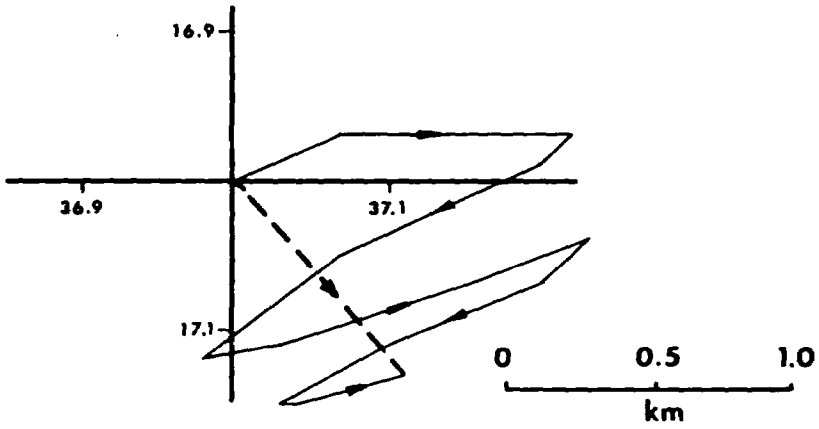

Figure 38 Movement of a water particle during one tidal cycle at Point 17 (location see Figure 1) (Wind 9m/sec, from SW)

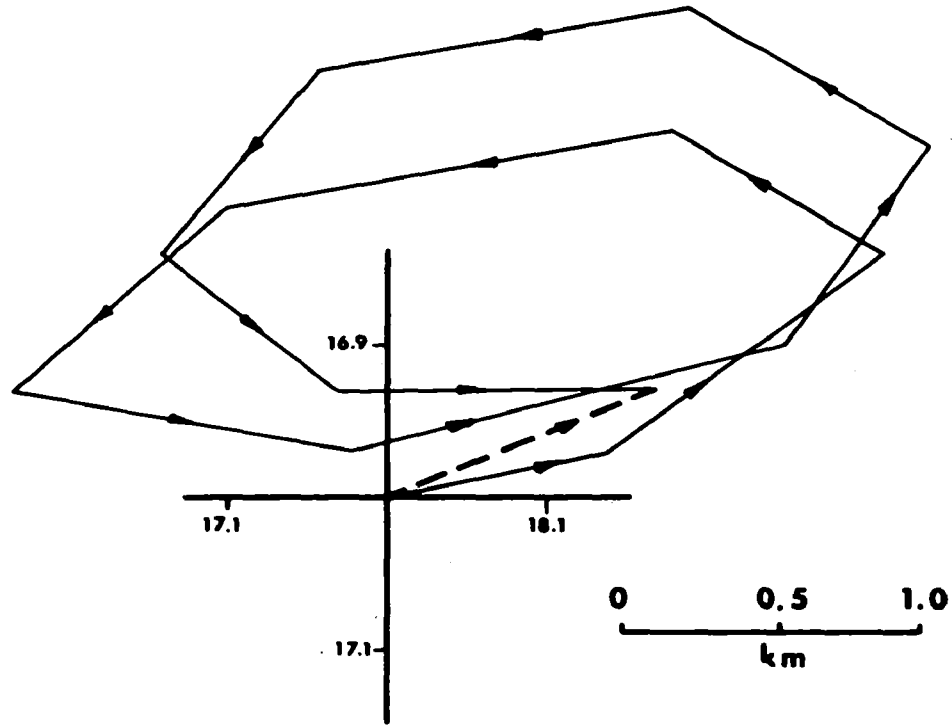

Figure 39 Movement of a water particle during one tidal cycle at Point 18 (location see Figure 1) (Wind 9m/sec, from SW)

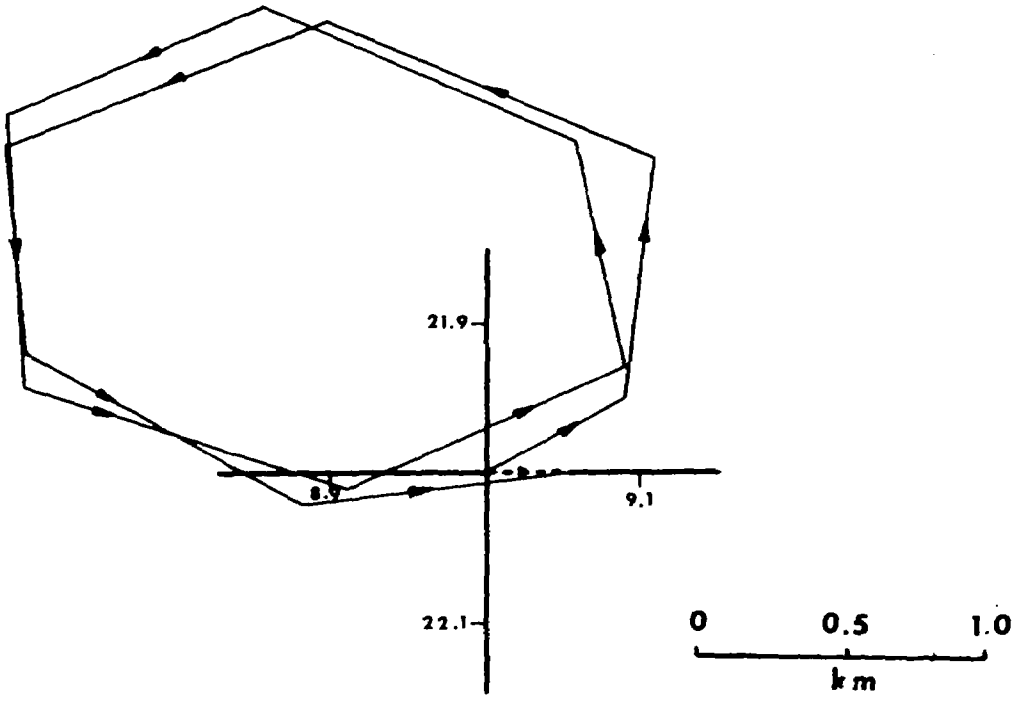

Figure 40 Movement of a water particle during one tidal cycle at Point 19 (location see Figure 1) (Wind 9m/sec, from SW)

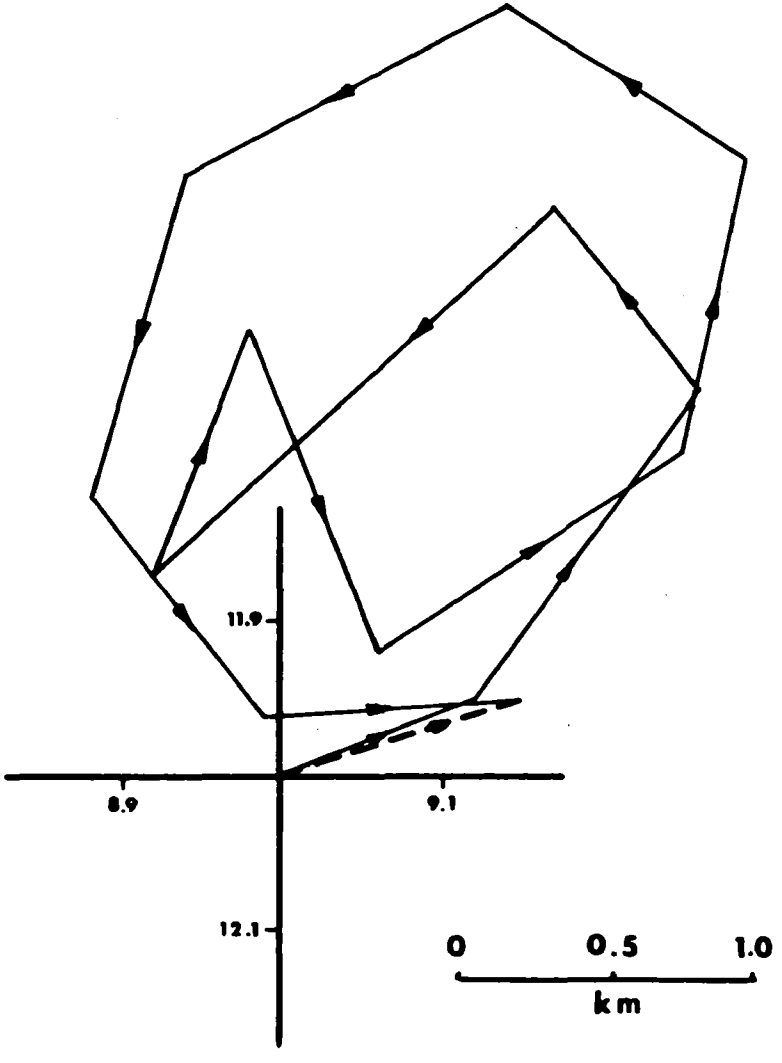

Figure 41 Movement of a water particle during one tidal cycle at Point 20 (location see Figure 1) (Wind 9m/sec,from SW)

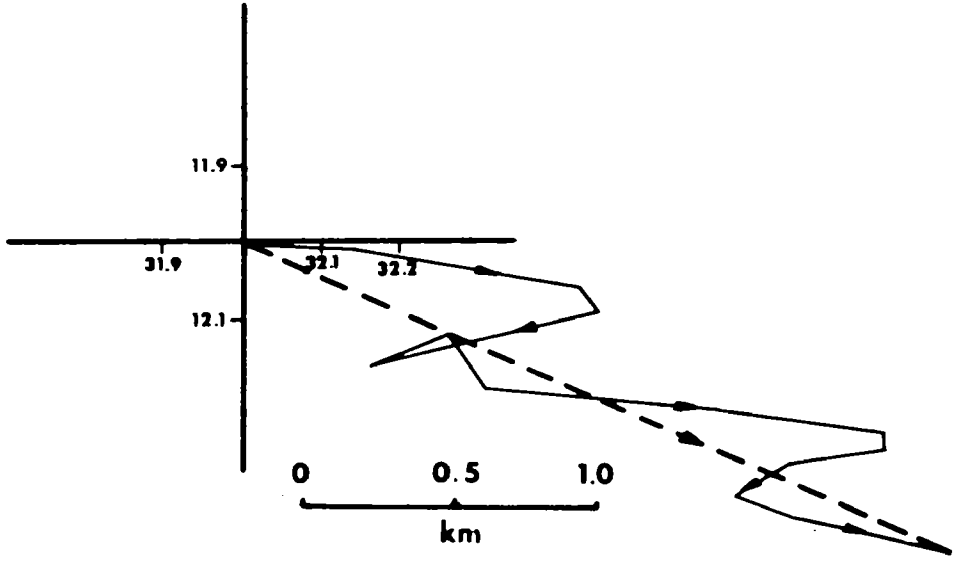

Figure 42 Movement of a water particle during one tidal cycle at Point 21 (location see Figure 1) (Wind 9m/sec, from SW)

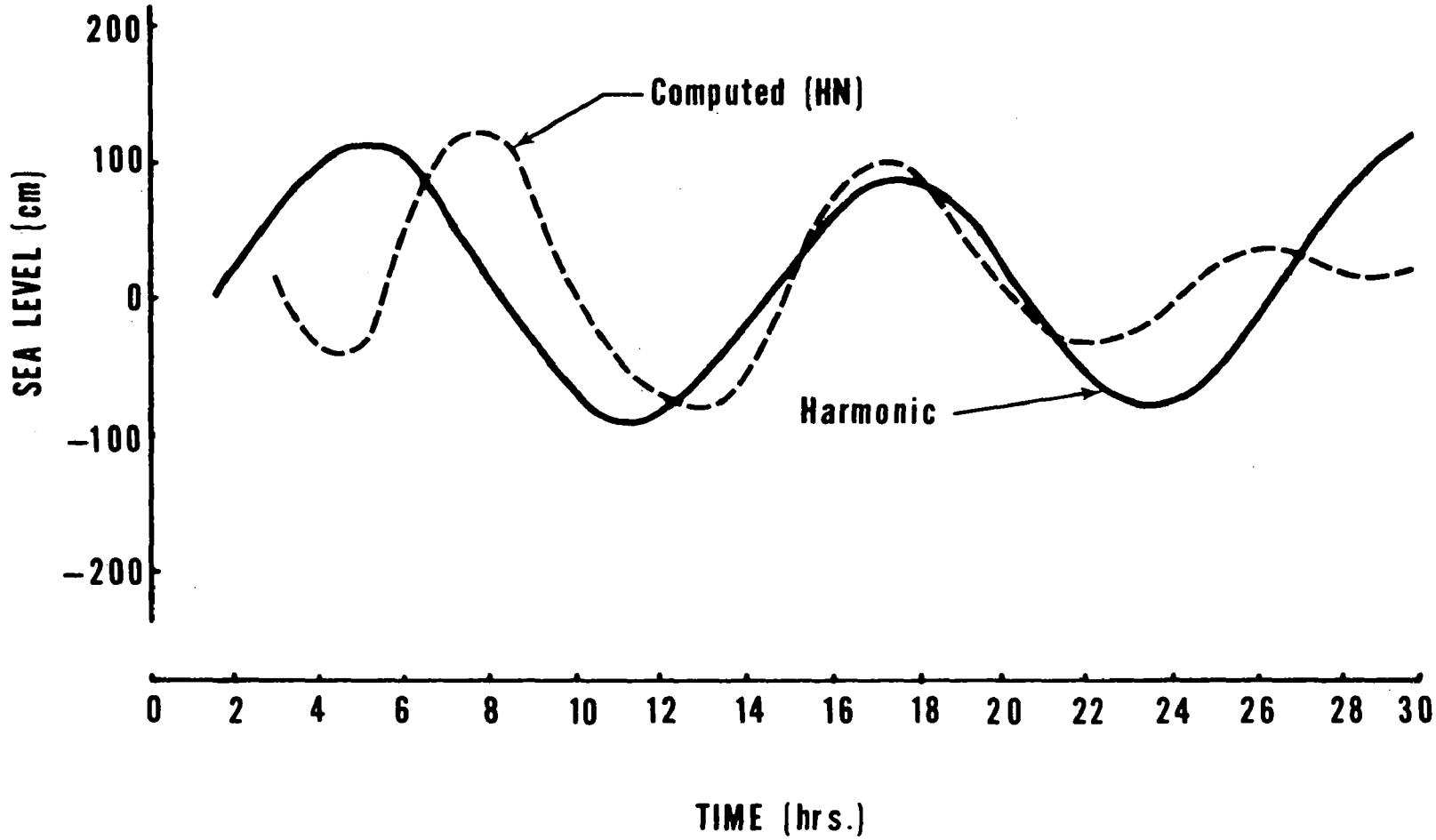

Figure 43 Comparison of sea level changes at Sandy Hook; A-computed with two-layer HN model; B-harmonic tidal predictions

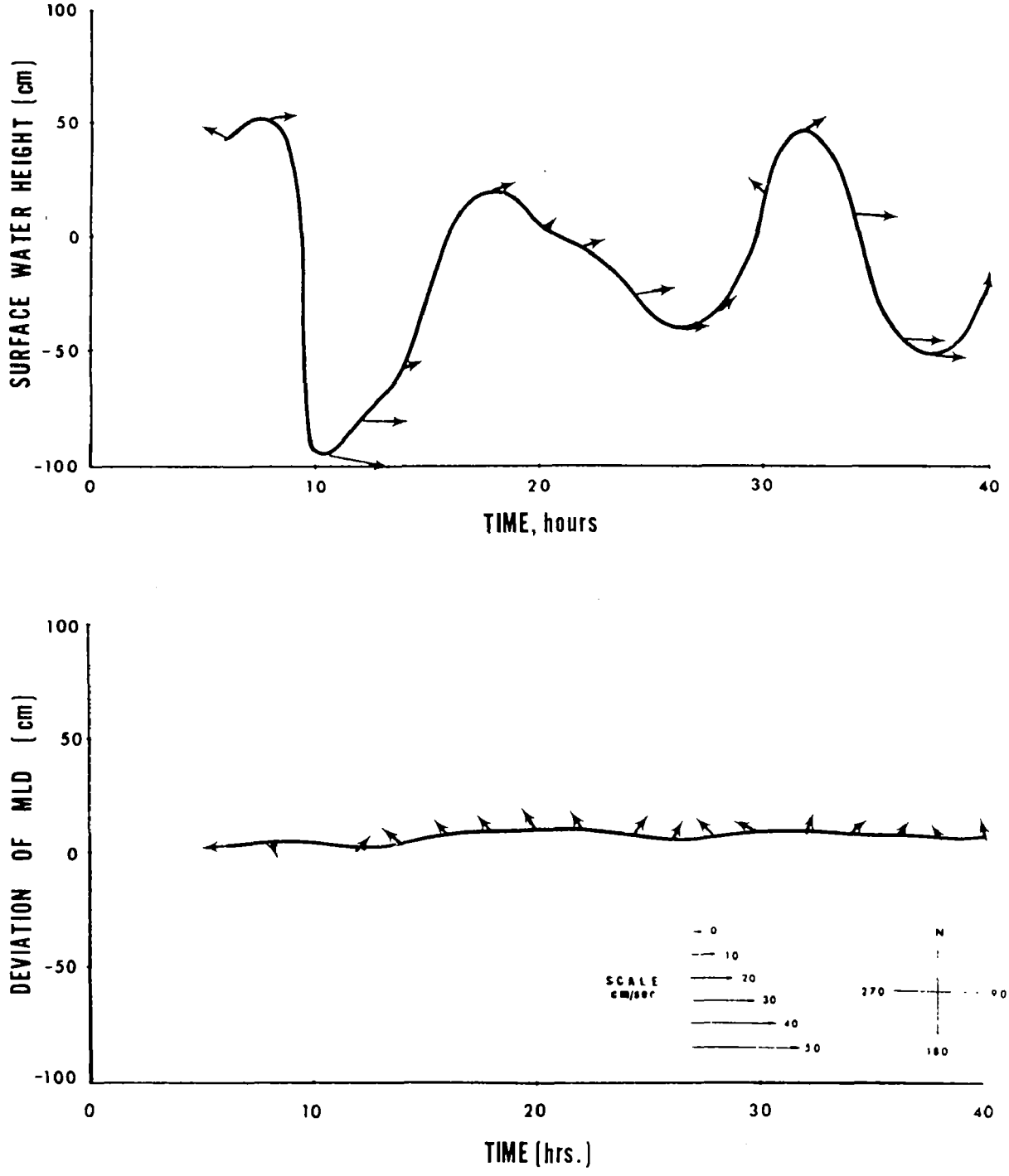

Figure 44 A Sea level changes and currents in upper layer at Point 5 (location see Figure 1) as computed with 2-layer HN model; wind 9m/sec^{-1} from SW.

B Change of mixed layer depth from mean and currents in lower layer at Point 5 (location and wind the same as for upper layer)

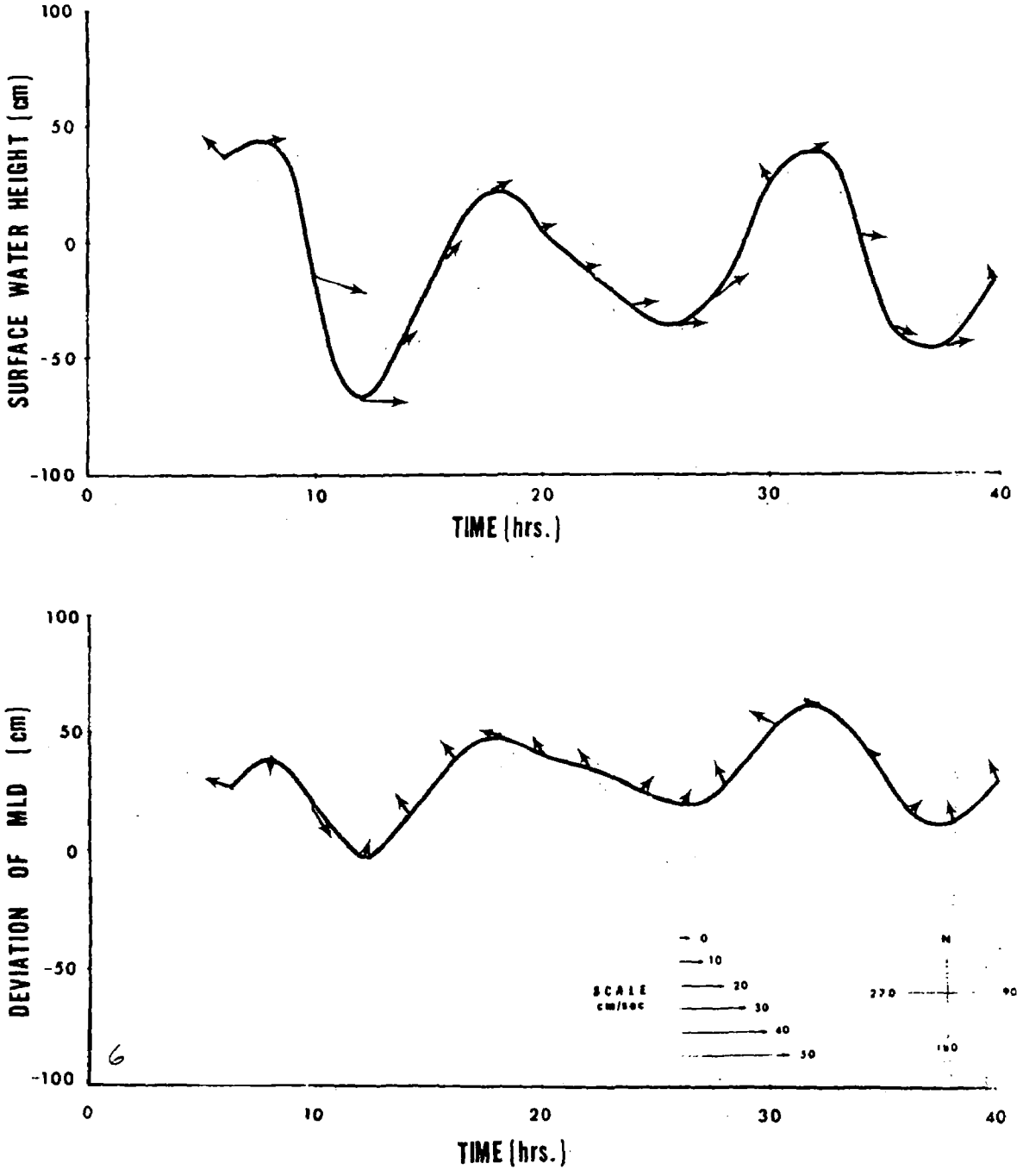

Figure 45 A Sea level changes and currents in upper layer at Point 7 (location see Figure 1) as computed with 2-layer HN model; wind 9m/sec^{-1} from SW

B Change of mixed layer depth from mean and currents in lower layer at Point 7 (location and wind the same as for upper layer)

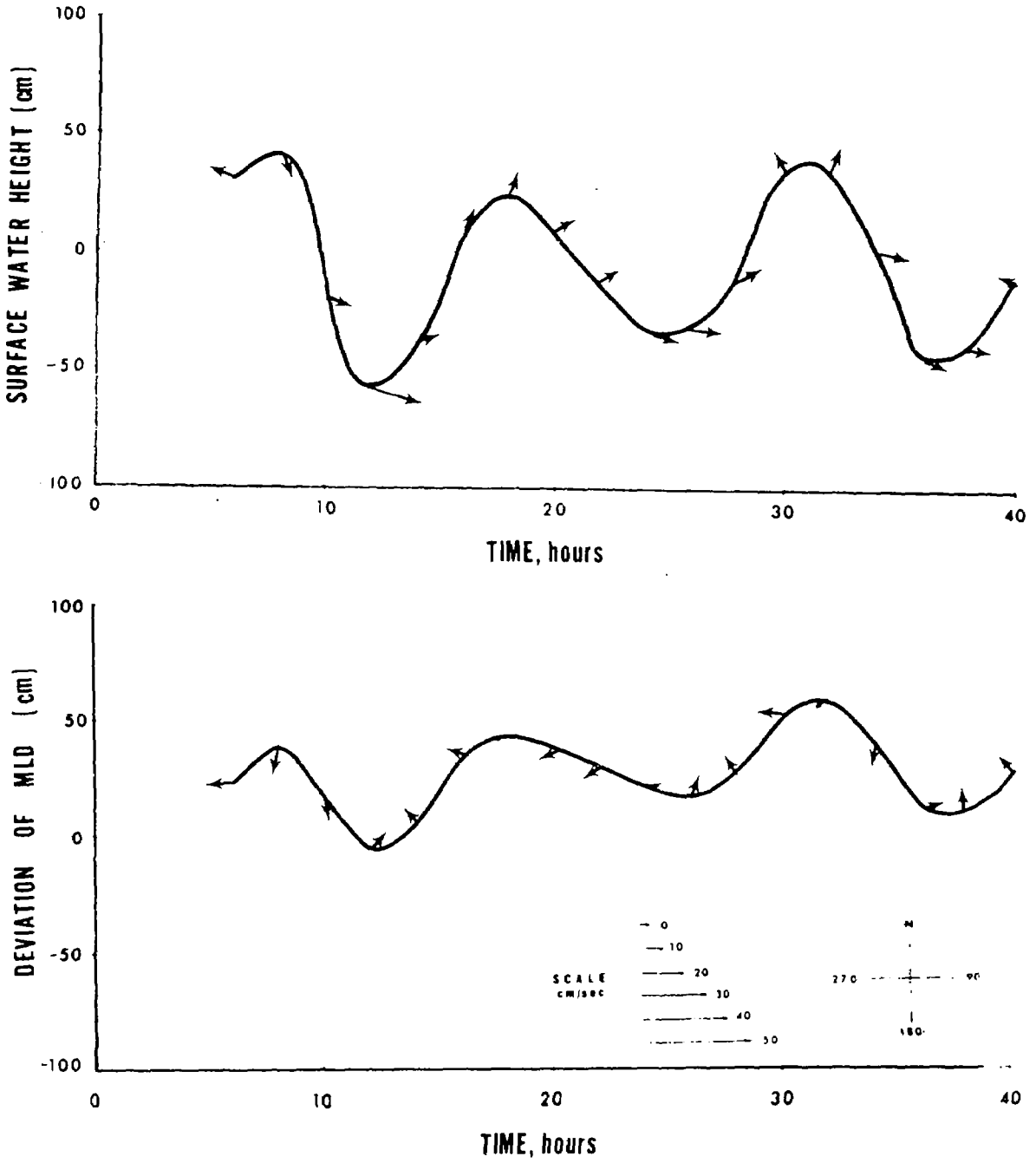

Figure 46 A Sea level changes and currents in upper layer at Point 10 (location see Figure 1) as computed with 2-layer HN model; wind 9m/sec^{-1} from SW

B Change of mixed layer depth from mean and currents in lower layer at Point 10 (location and wind the same as for upper layer)

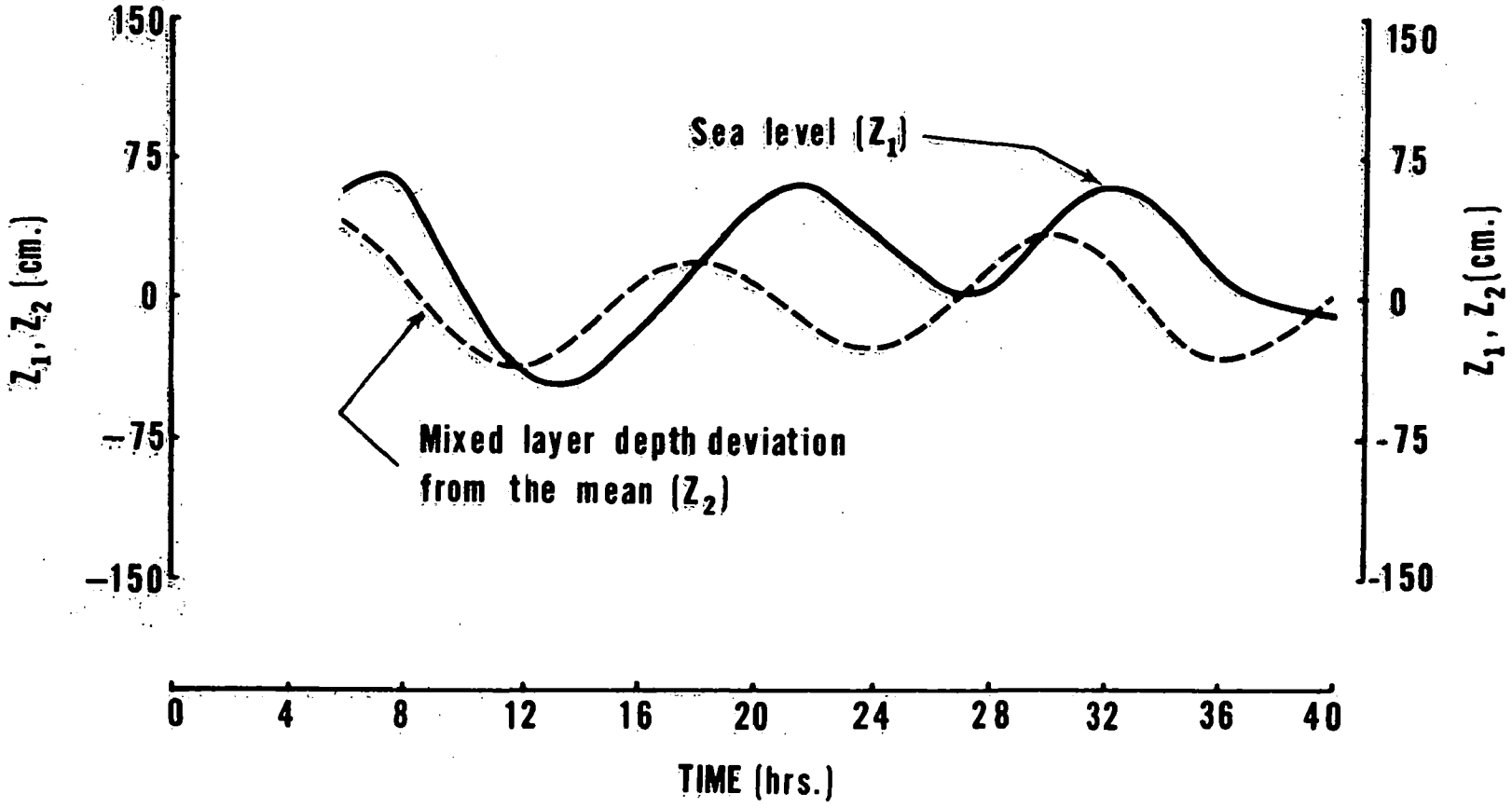

Figure 47 Change of sea level and mixed layer depth change at Point 20 (location see Figure 1)

AMBROSE CHANNEL LIGHTSHIP

(40°28.0'N - 73°50.0W)

CURRENT COMPUTED AT GRID

23,37

Figure 48 Mean tidal currents at Ambrose Channel Lightship (40°28.0'N, 73°50.0'W) (from Haight, 1942) and currents in upper layer computed with HN model at grid 23,37; wind 9m sec^{-1} from SW

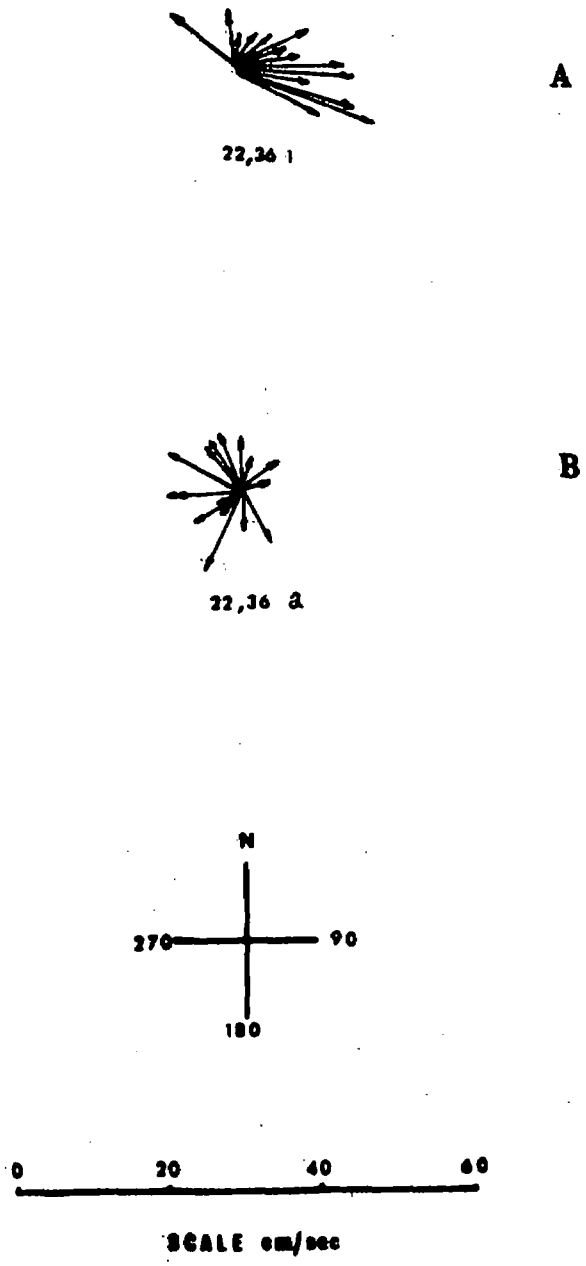

Figure 49 Currents at Point 5 (location see Figure 1) A: upper layer; B: lower layer. Wind 9m sec^{-1} from SW

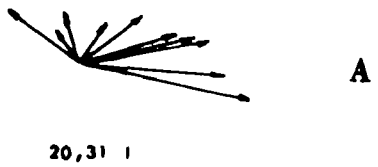

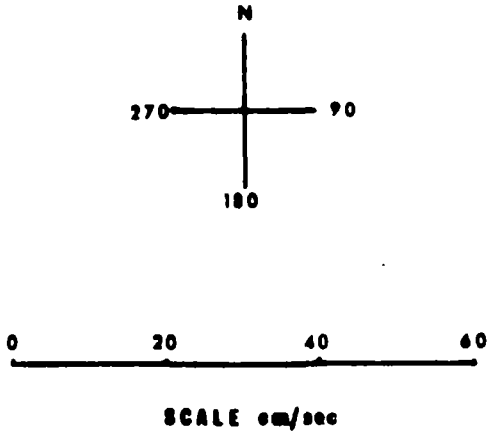

Figure 50 Currents at Point 7 (location see Figure 1) A: upper layer; B: lower layer. Wind 9m sec^{-1} from SW

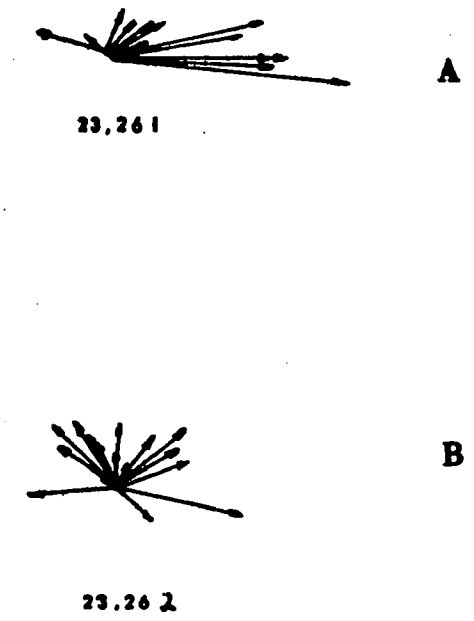

Figure 51 Currents at Point 10 (location see Figure 1) A; upper layer; B: lower layer, Wind 9m sec^{-1} from SW

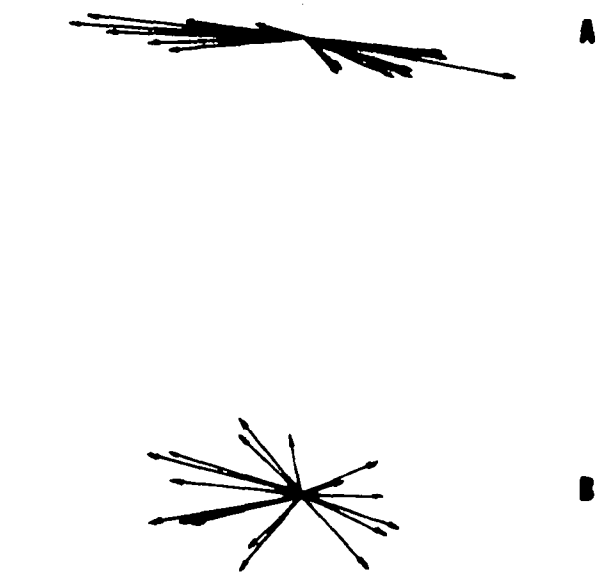

Figure 52 Currents at Point 12 (location see Figure 1) A: upper layer; B: lower layer. Wind 9m sec^{-1} from SW

Figure 53 Currents at Point 13 (location see Figure 1) A: upper layer; B: lower layer. Wind 9m sec^{-1} from SW

Figure 54 Currents at Point 14 (location see Figure 1) A: upper layer; B: lower layer. Wind 9m sec^{-1} from SW

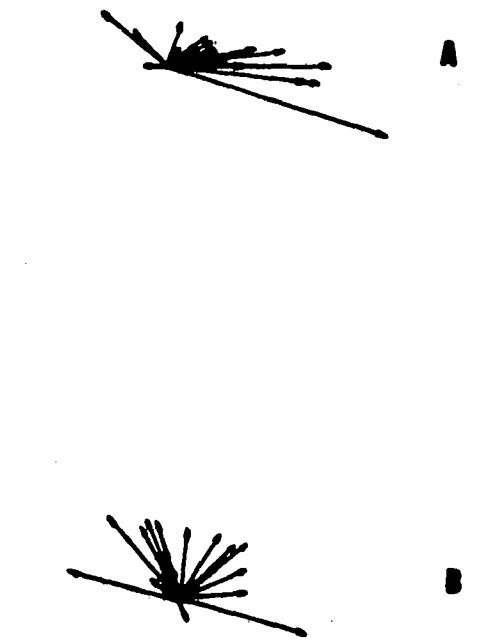

Figure 55 Currents at Point 15 (location see Figure 1) A: upper layer; B: lower layer. Wind 9m sec^{-1} from SW

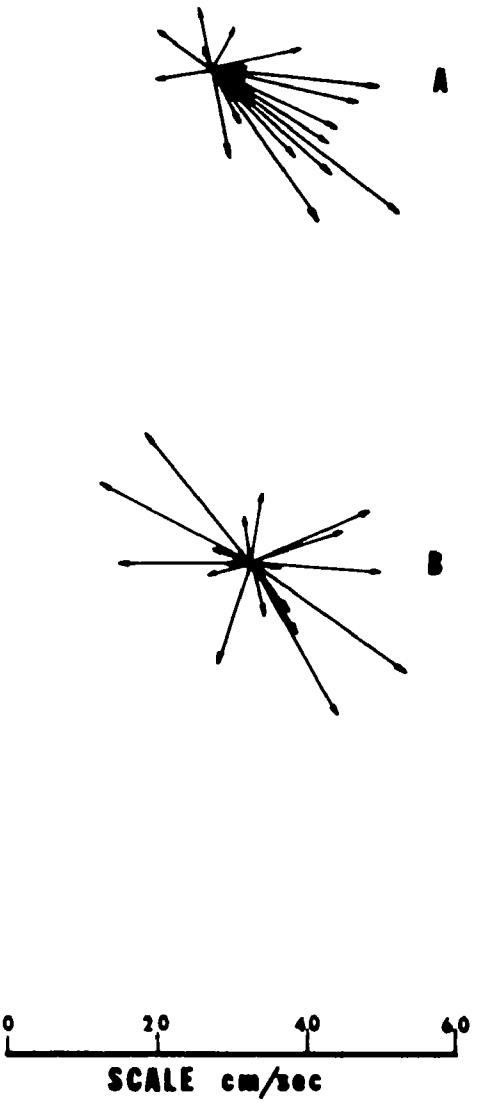

Figure 56 Currents at Point 20 (location see Figure 1) A: upper layer; B: lower layer. Wind 9m sec^{-1} from SW

Figure 57 Currents at Point 24 (location see Figure 1) A: upper layer; B: lower layer. Wind 9m sec^{-1} from SW

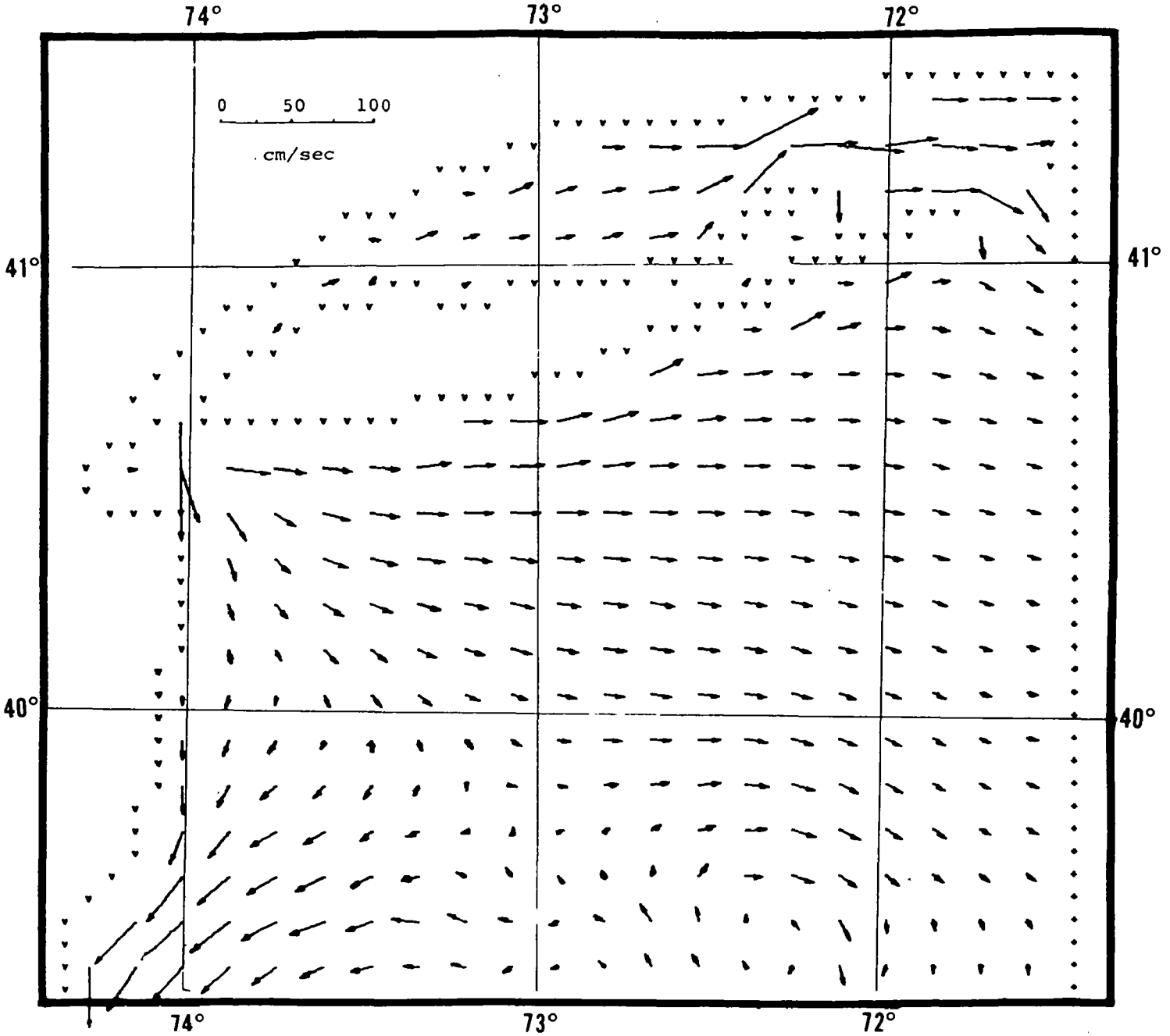

Figure 58 Currents in surface layer at low water at Sandy Hook (wind 9m sec^{-1} from SW)

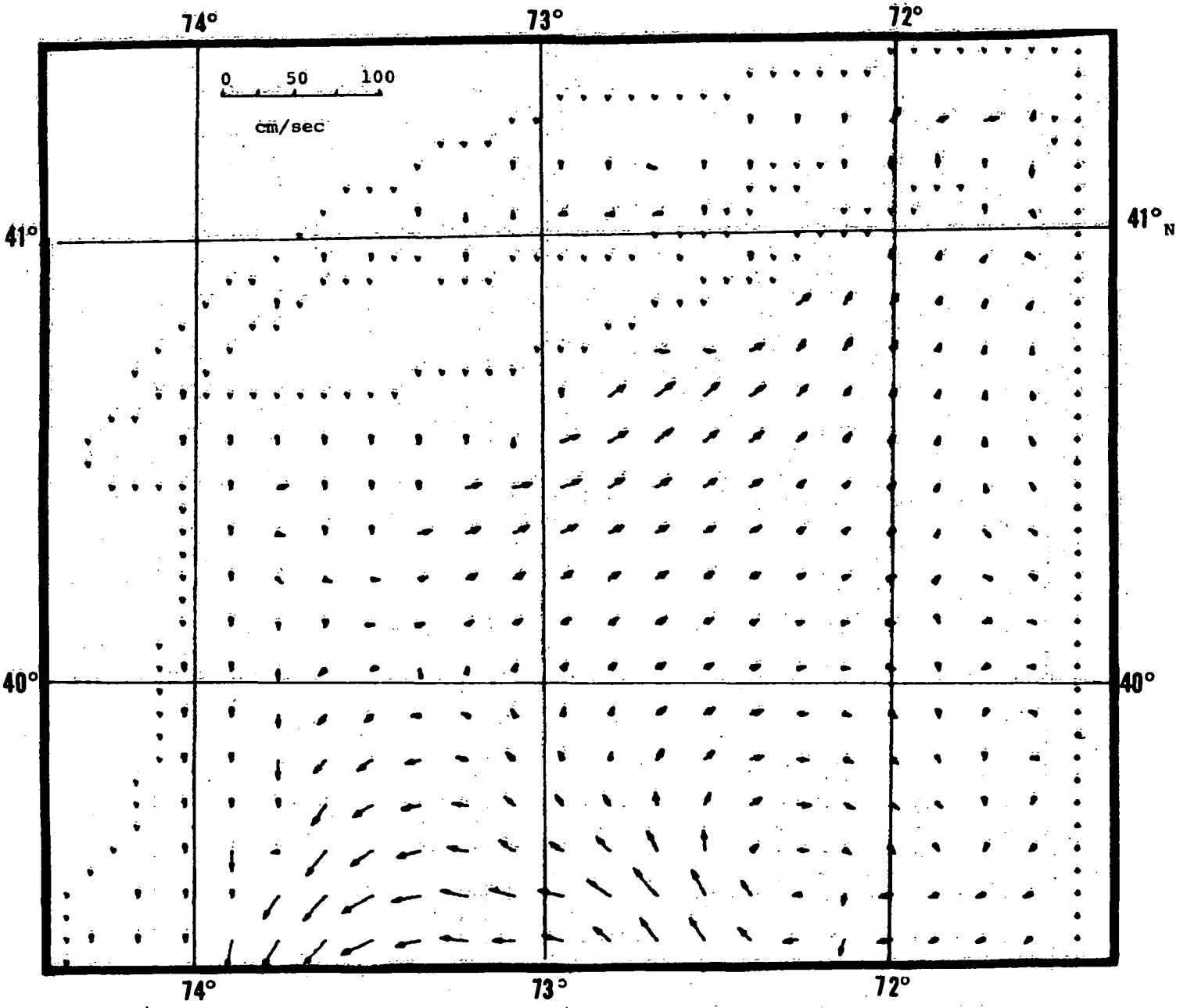

Figure 59 Currents in bottom layer at low water at Sandy Hook (wind 9m sec^{-1} from SW)

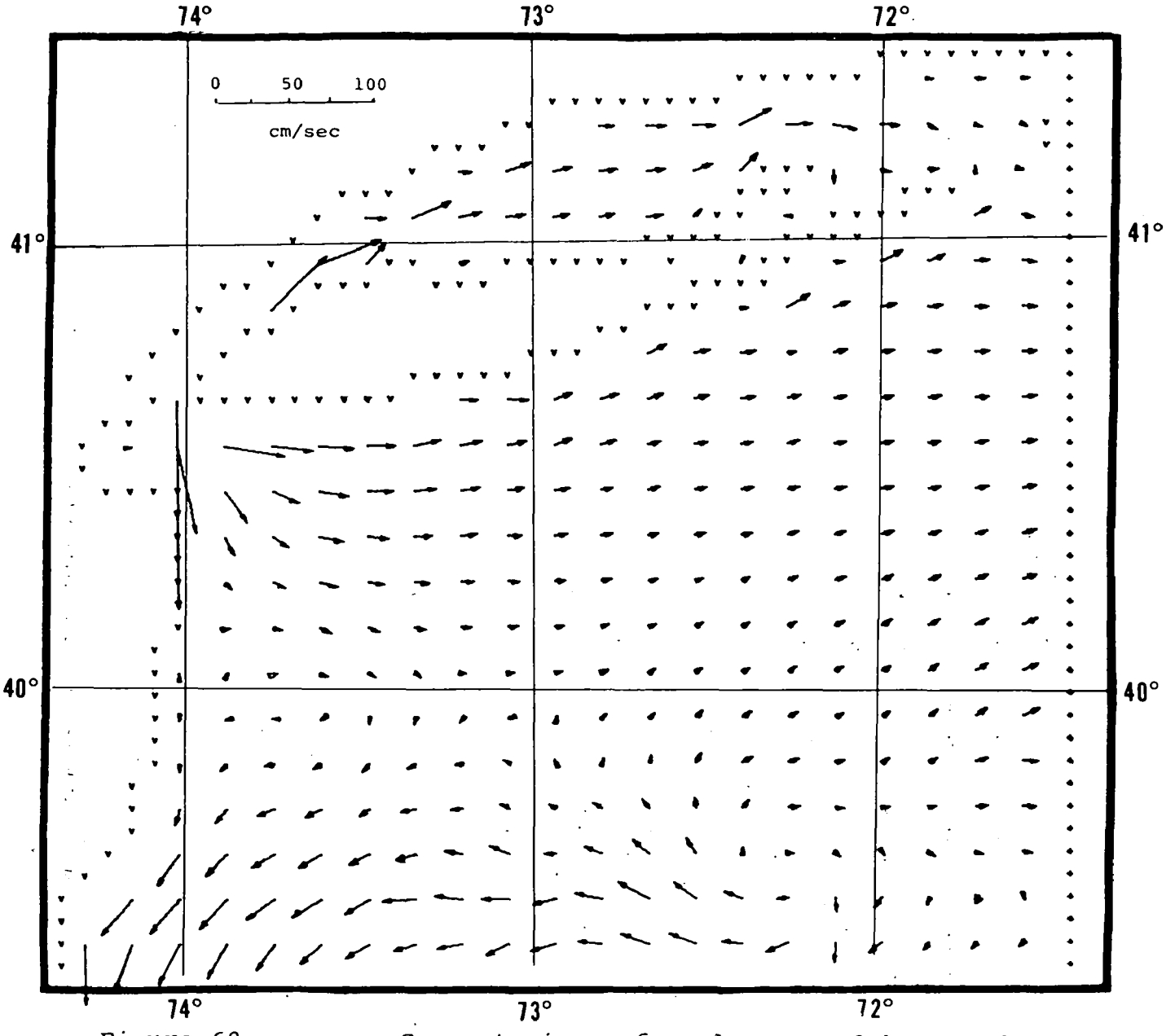

Figure 60 Currents in surface layer at 2 hours after low water in Sandy Hook (wind 9m sec^{-1} from SW)

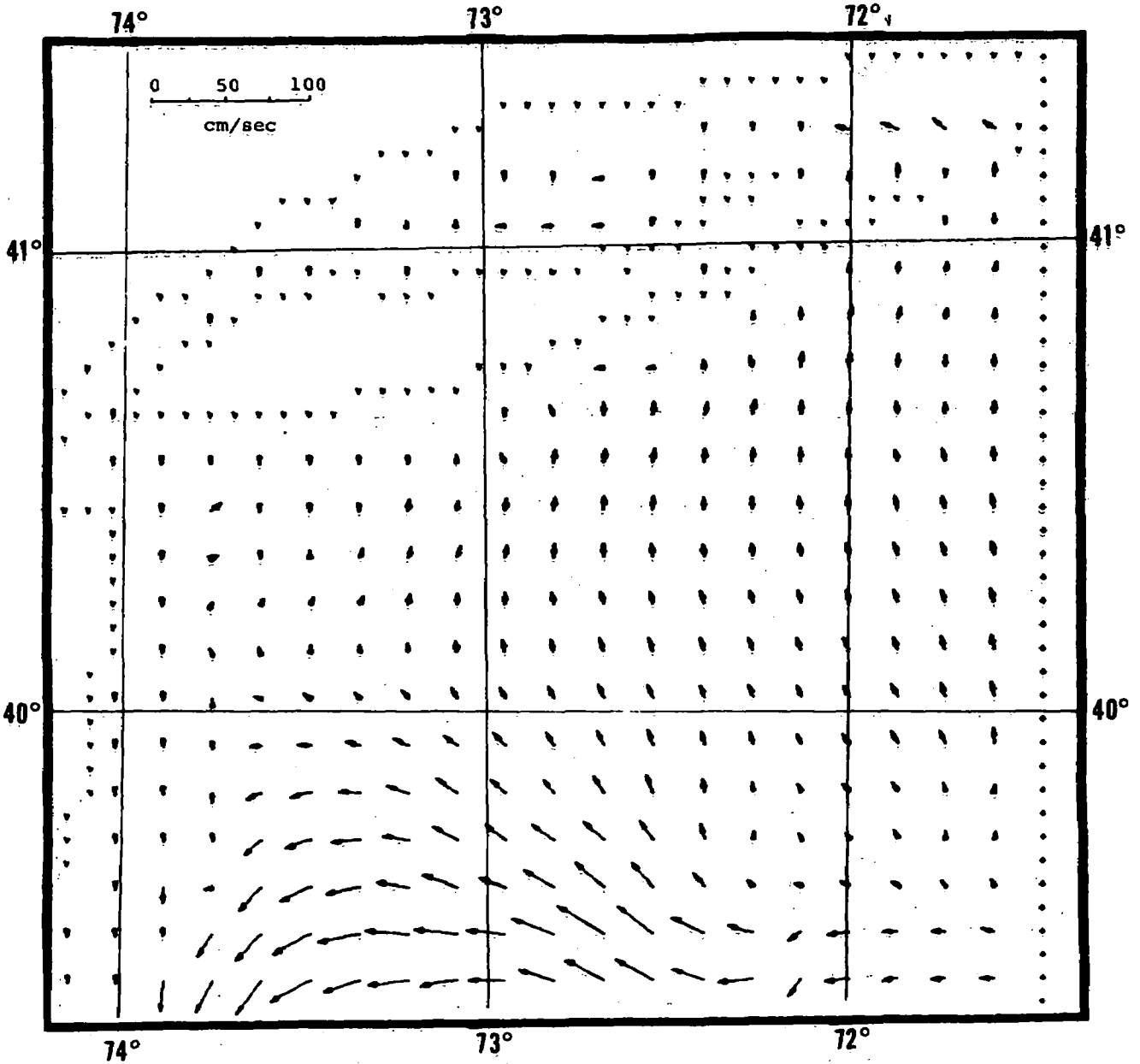

Figure 61 Currents in bottom layer at 2 hours after low water at Sandy Hook (wind 9m sec^{-1} from SW)

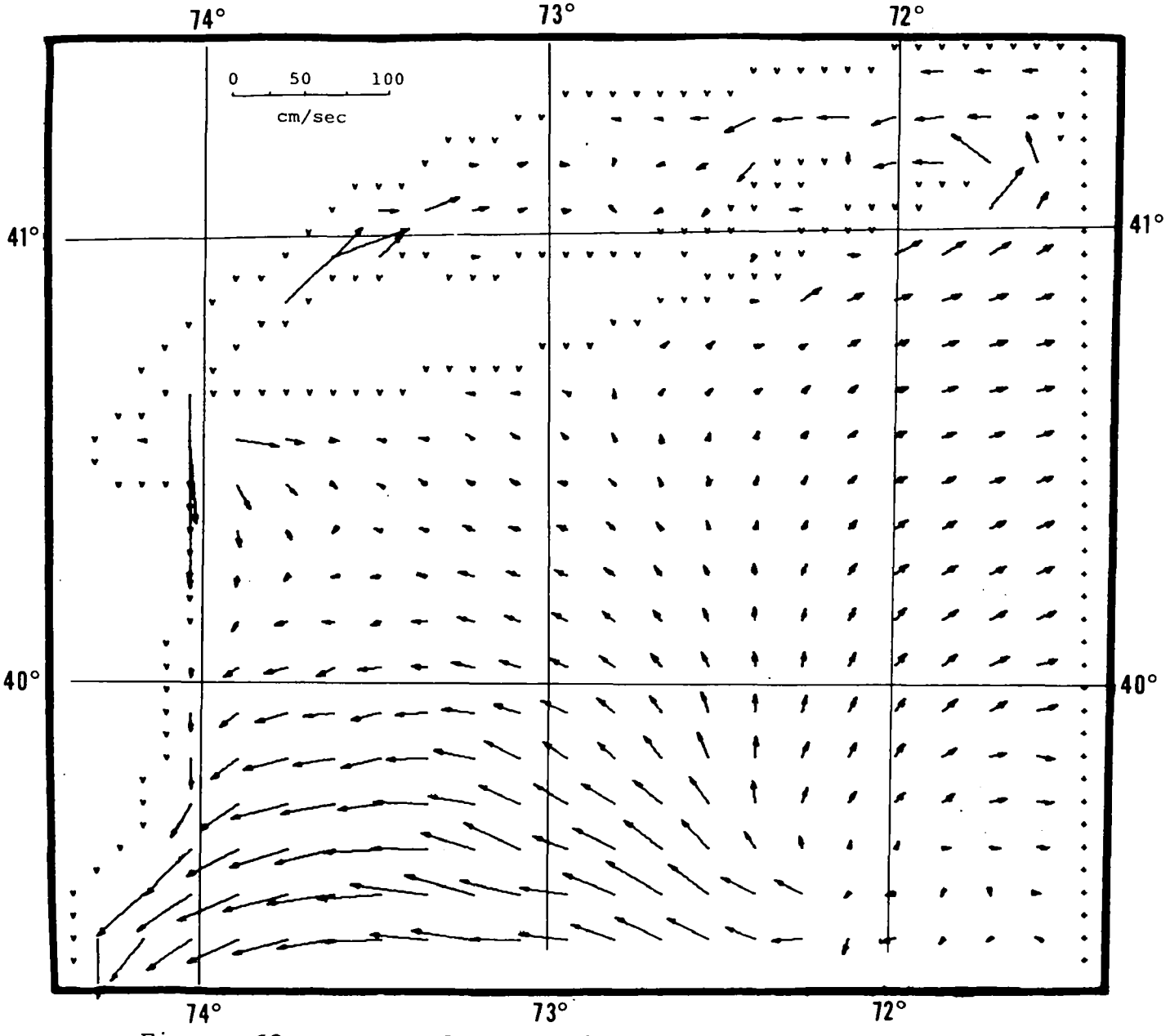

Figure 62 Currents in surface layer 2 hours before high water at Sandy Hook (wind 9m sec^{-1} from SW)

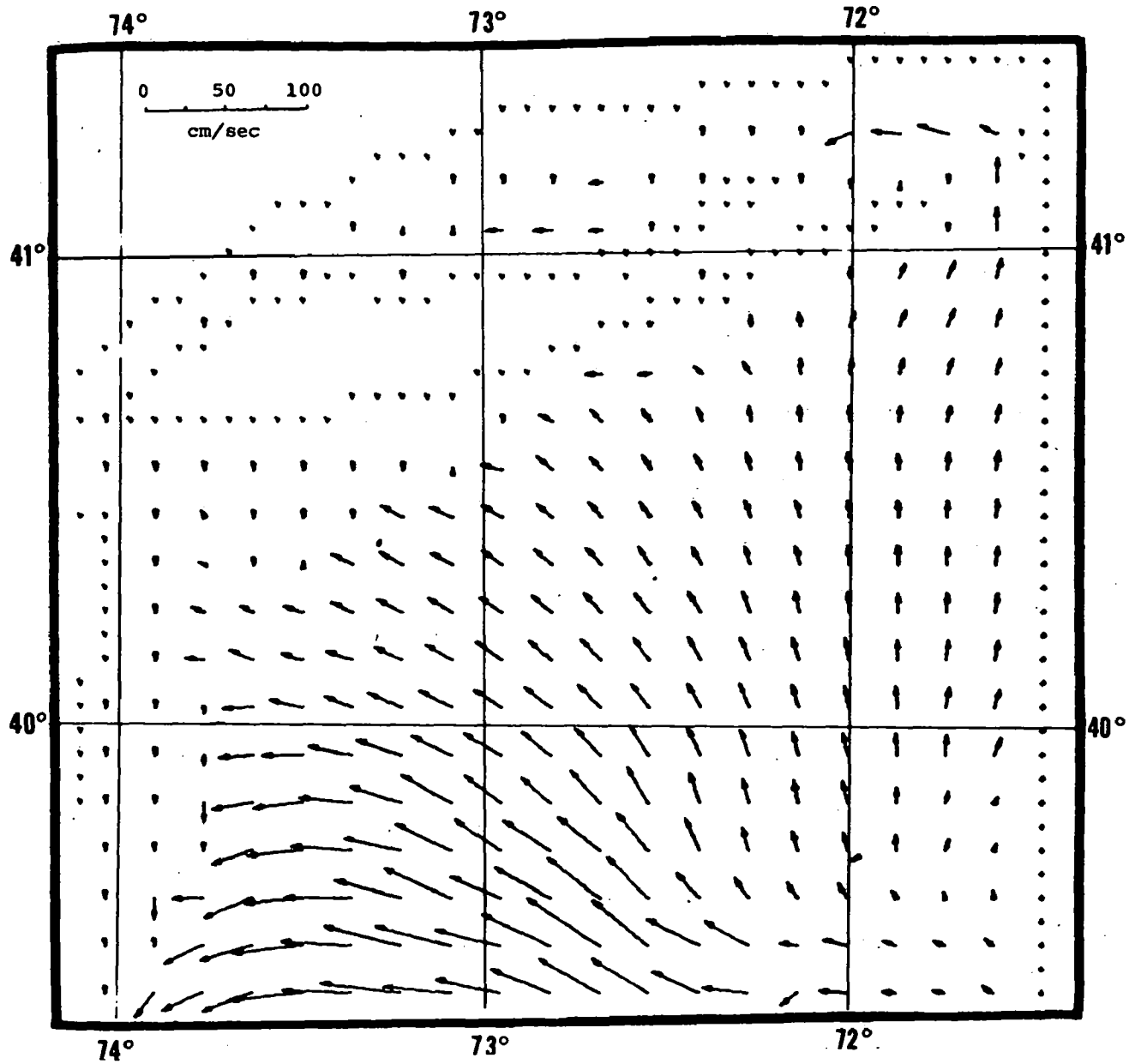

Figure 63 Currents in bottom layer 2 hours before high water at Sandy Hook (wind 9m sec^{-1} from SW)

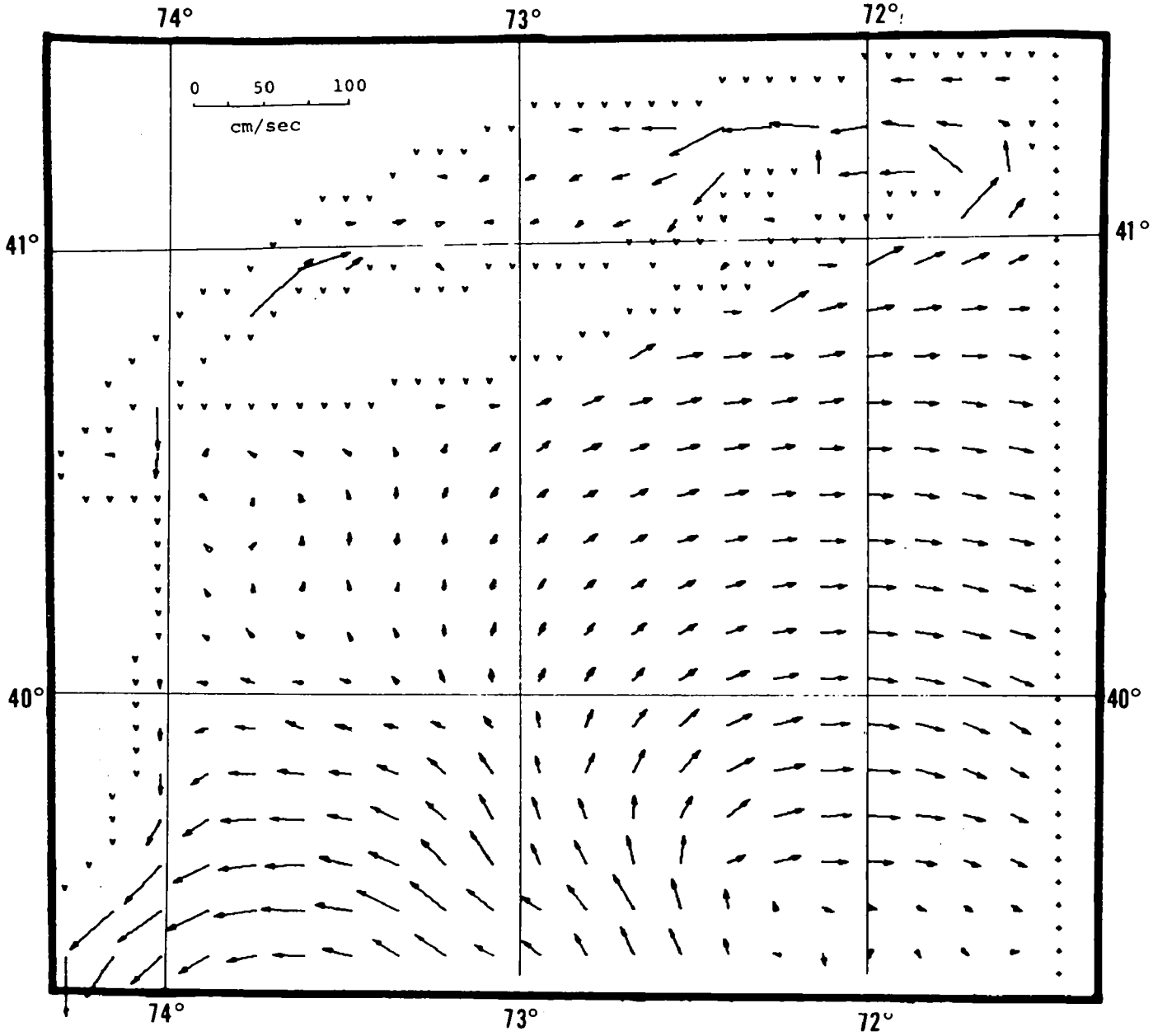

Figure 64 Currents in surface layer at high water at Sandy Hook (wind 9m sec^{-1} from SW)

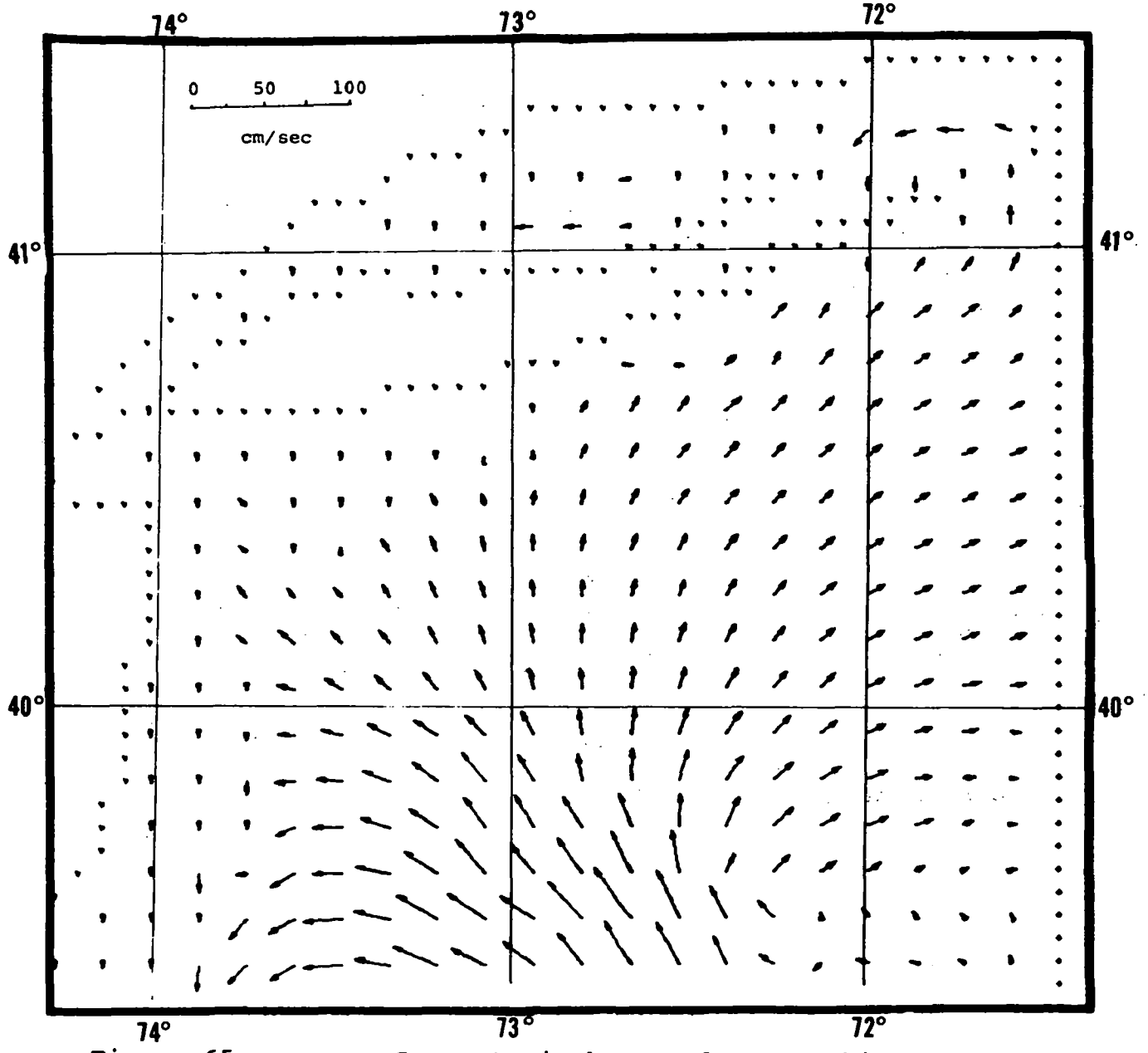

Figure 65 Currents in bottom layer at high water at Sandy Hook (wind 9m sec^{-1} from SW)

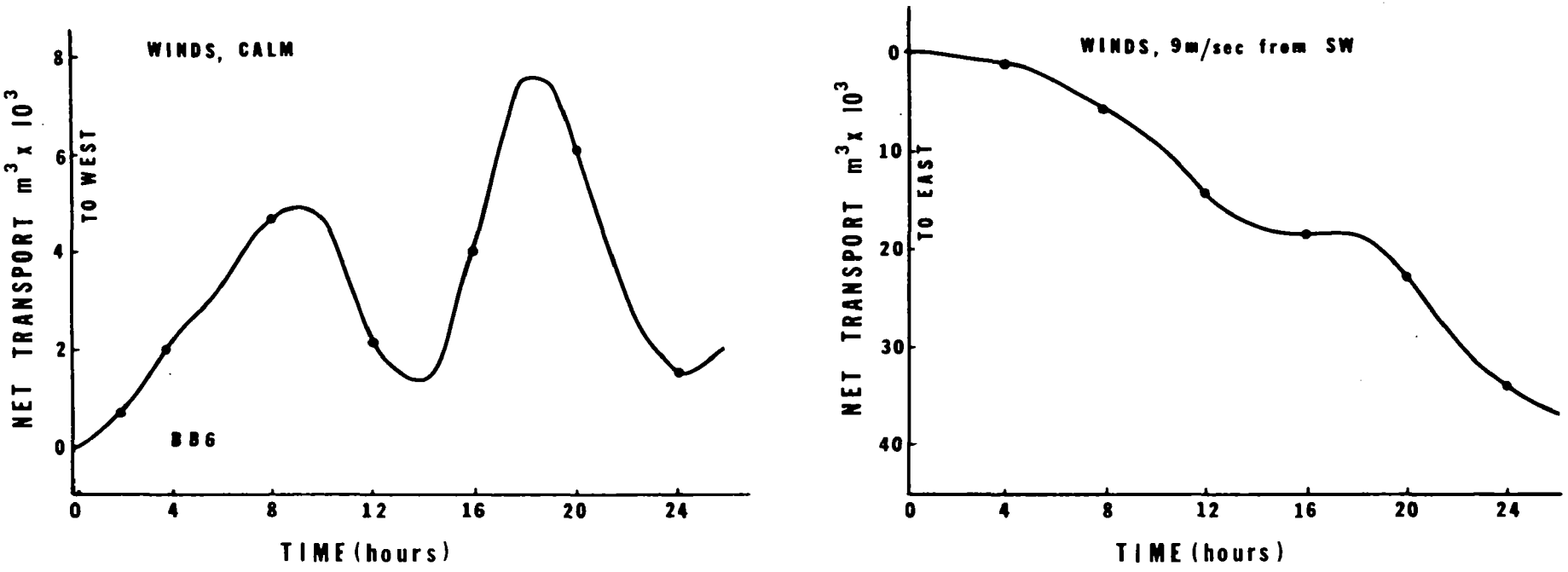

Figure 66 Transport rate through section BB6 in surface layer in calm and with SW wind 9m/sec.

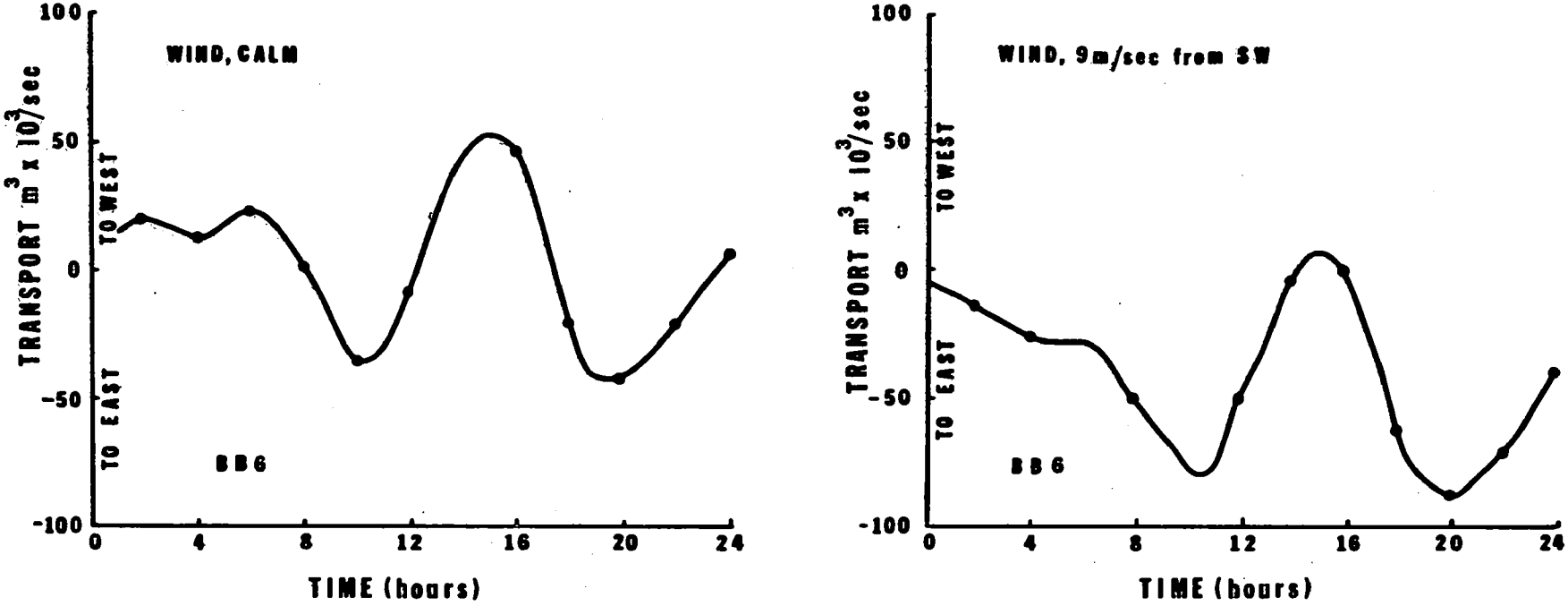

Figure 67 Net Transport through section BB6 in calm and with SW winds 9m/sec.

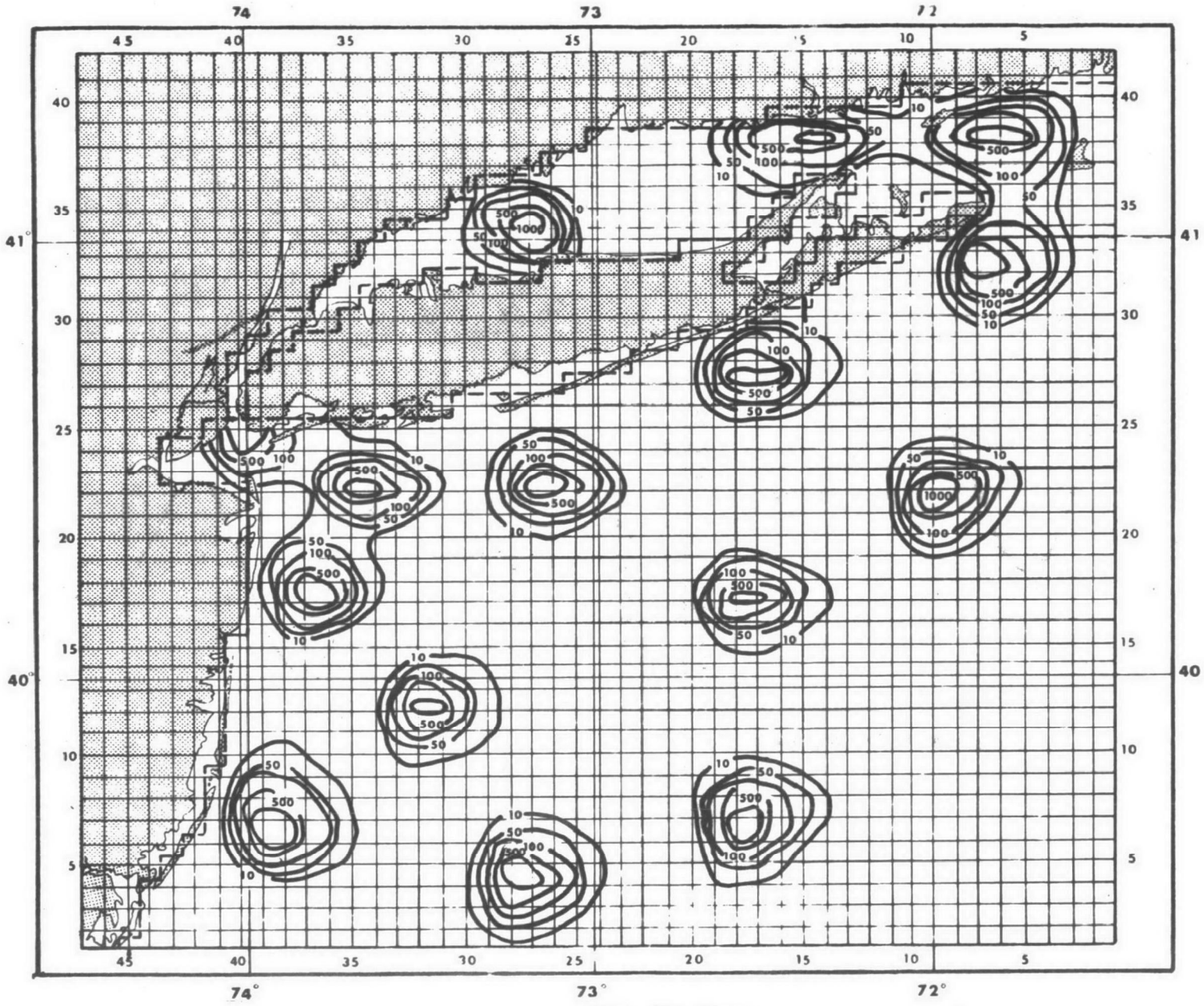

Figure 68 Computed concentrations 24 hours after release.

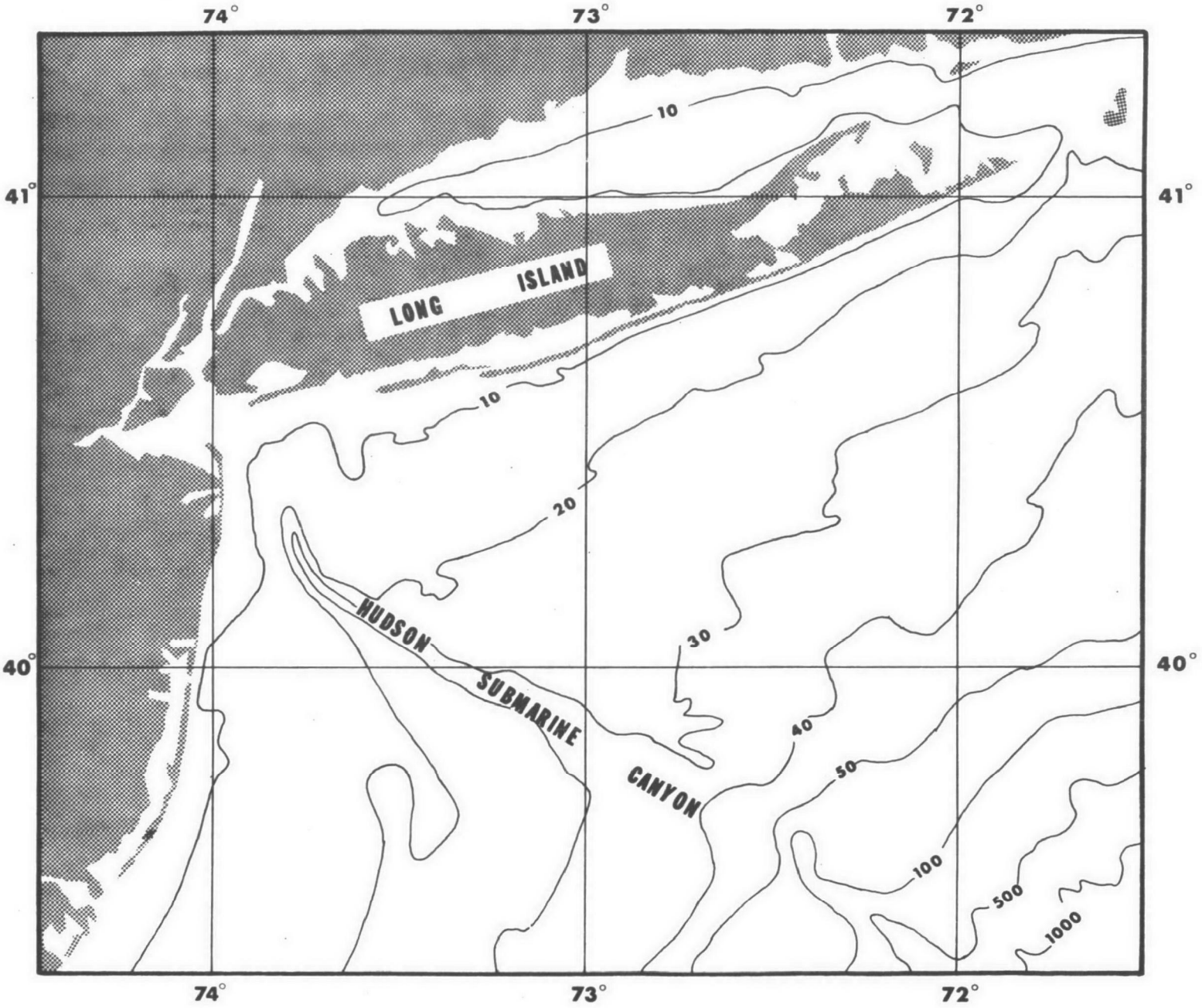

Figure 69 Bathymetric charts of New York Bight (isobaths in fathoms)